universität wien

MASTERARBEIT | MASTER'S THESIS

Titel | Title

Metabolomics and Proteomics Analysis of M1 and M2 Macrophages - Evaluation of the Effects of a Mitochondrial Damaging Agent on the Metabolism of Macrophages

verfasst von | submitted by

Alexander Henry Kozan B.Sc.

angestrebter akademischer Grad | in partial fulfilment of the requirements for the degree of

Master of Science (MSc)

Wien | Vienna, 2026

Studienkennzahl lt. Studienblatt | Degree programme code as it appears on the student record sheet:	UA 066 606
Studienrichtung lt. Studienblatt | Degree programme as it appears on the student record sheet:	Masterstudium Drug Discovery and Development
Betreut von | Supervisor:	Dr. Astrid Slany Privatdoz.

Acknowledgments

I would like to thank Dr. Astrid Slany, who made it possible for me to conduct the work for my master's thesis in the Gerner Lab and who's supervision made this thesis possible, thanks to her guidance not only for this work but my academic development in general.

I am also grateful for my parents, for encouraging me to chase my scientific career, for their enduring support and to whom I am forever indebted.

I want to thank Nora, for always keeping my spirits up.

Lastly, I would like to thank Ines, who helped me make decisions, gave me strength and who acted as a haven of tranquility I could retreat to after a long day in the lab.

Contents

List of Figures

List of Tables

Abstract

Cancer is an ongoing detriment to public health with available treatment options still leaving much to be desired. The reason for this, is the complexity and heterogeneity of this disease group, with hallmarks spanning across multiple biological functions, which aren't all addressed with current therapies. One of the factors playing into cancer progression is the tumor microenvironment (TME). In the TME there are multiple cell types that assist tumors in their growth, such as macrophages, called tumor associated macrophages (TAMs). These support cancer malignancy through pathways associated with the M2 macrophage polarization state. Macrophages can achieve a plethora of biological functions through polarization into different states, for instance the pro-inflammatory M1-like phenotype opposing the anti-inflammatory M2-like phenotype. Understanding the cellular polarization mechanisms is of importance to discover novel cancer treatments. These may address the supporting role of the TAMs in the TME or use the anti-cancer function of M1 macrophages as immunotherapy. In this work, the metabolic and proteomic signatures of macrophage polarization were studied by differentiating U937 cells into M0-, M1-, and M2 macrophages then subsequently analyzing the metabolome and proteome using LC-MS techniques. Additionally, the effect of an oxidative environment on the metabolome of the macrophages was investigated by treating the different cell types with tert-butyl hydroperoxide (TBHP), since reactive oxygen species (ROS) play a role in the cellular functions of macrophages as well as in inflamed tissue. The LC-MS analysis showed clear metabolic differences between the differently polarized macrophages that were confirmed with the expression profiles of respective proteins. The plasticity of macrophages was demonstrated by the fact that a mix of pro- and anti-inflammatory pathways were found in the same cell. Additionally, TBHP treatment had an impact on certain metabolites, namely dihydroxyacetone phosphate, fructose-1,6-biphosphate, 3-hydroxyanthranilic acid and orotic acid.

Zusammenfassung

Krebs stellt eine aktuelle Bedrohung der öffentlichen Gesundheit dar, wobei die bestehenden Therapiemöglichkeiten noch Platz für Verbesserungen lassen. Der Grund dafür ist die Komplexität und Heterogenität dieser Krankheitsgruppe. Krebsentstehung und Wachstum ist nämlich tief verwurzelt in vielen biologischen Prozessen, welche aber nicht immer von den derzeitigen Behandlungen addressiert werden. Ein Faktor der zum Krankheitsverlauf beiträgt, ist die Tumormikroumgebung, in der verschiedene Zellarten Krebs auf unterschiedliche Art und Weise unterstützen können. Eine davon sind zum Beispiel die Tumor-assoziierten Makrophagen (TAM), die durch Funktionen des M2 Polarisierungszustands zur Bösartigkeit von Tumoren beitragen. Makrophagen können eine Vielzahl an biologischen Funktionen erfüllen durch Polarisierung zu verschiedenen Zuständen, beispielsweise die pro-entzündlichen M1 Makrophagen, die den anti-entzündlichen M2 Makrophagen gegenüberstehen. Es ist von Bedeutung die Mechanismen, die hinter der Makrophagenpolarisierung stecken, zu verstehen, um neue Krebstherapien zu entwickeln. Diese könnten nämlich die unterstützende Rolle der TAM addressieren, oder die antitumorale Eigenschaften des M1 Phänotyps in Immuntherapien anwenden. In dieser Arbeit wurden die Unterschiede zwischen den verschiedenen Polarisierungszuständen auf metabolischer und proteomischer Ebene untersucht, indem U937 Zellen zu M0-, M1- und M2 Makrophagen differenziert wurden mit anschließender LC-MS Analyse des Metaboloms und Proteoms. Zusätzlich wurde der Effekt von oxidativem Stress auf das Metabolom der unterschiedlich polarisierten Makrophagen untersucht, indem die Zellen mit tert-Butylhydroperoxid (TBHP) behandelt wurden. Reaktive Sauerstoffspezies spielen nämlich in den natürlichen Zellfunktionen von Makrophagen und in entzündetem Gewebe eine Rolle. Die LC-MS Analyse zeigte klare metabolische Unterschiede zwischen den verschiedenen Makrophagen-Typen, die mit der Expression von bestimmten Proteinen verifiziert wurden. Die Plastizität der Makrophagen wurde dadurch veranschaulicht, dass eine Mischung aus pro- und anti-entzündlichen Stoffwechselwegen in der gleichen Zelle gefunden wurden. Die TBHP Behandlung zeigte Auswirkung auf bestimmte Metabolite, nämlich Dihydroxyacetonphosphat, Fructose-1,6-bisphosphat, 3-Hydroxyanthranilsäure und Orotsäure.

1 Introduction

1.1 Macrophage Function in Immune Response

Macrophages are myeloid immune cells with the ability to clear dying cells as well as pathogens from the human organism through phagocytosis and modulation of inflammatory response [1]. Macrophages are part of the innate immune system [2] and protect against infections, maintain tissue homeostasis as well as mediate inflammation [3]. They can derive from monocytes migrating from the blood into tissue [4] or can be tissue-resident macrophages that develop in embryonic stages and remain locally throughout life [3]. Yet macrophages are to be seen as plastic cells due to their high diversity in tissue-specific functionality [5]. As cells with high plasticity and high diversity, macrophages can be categorized into two cell states, namely M1 and M2 macrophages. While the M1-like subset is pro-inflammatory the alternatively activated M2-like macrophages act immunoregulatory and anti-inflammatory [6]. The former are derived from macrophages exposed to a pathogen associated molecular pattern such as lipopolysaccheride (LPS) originating from bacteria [7] alone or in combination with Th1 cytokines, like interferon (INF)-γ and granulocyte-macrophage colony-stimulating factor (GM-CSF). The latter differentiate through Th2 cytokine signaling, induced e.g. by interleukin (IL)-4 and IL-13. M1 macrophages initiate and sustain inflammation by producing pro-inflammatory cytokines such as IL-1β and tumor necrosis factor-α (TNF-α). Prolonged M1 signaling can lead to tissue damage. To prevent this, the ratio of phenotypes shifts towards macrophages exhibiting increased M2 polarization. In the M2 state, macrophages can halt the inflammatory response, by secreting immunosuppressive cytokines, such as IL-10 and transforming growth factor beta (TGF-β), as well as initiate tissue repair [8].

Macrophages produce reactive oxygen species (ROS) as part of their phagocytic mechanisms to defend against invading pathogens [9]. As a consequence, they reside in environments with high levels of oxidative stress factors [10] and have thus developed mechanisms for self-protection against ROS [9][10]. Yet the two polarization states differ in their respective ROS profiles [11]. On the one hand M1 macrophages produce ROS during phagocytosis in order to kill pathogens using respiratory burst [12]. On the other hand M2 macrophages utilize ROS to clear inflammation through efferocytosis [13][14][15]. Interestingly efferocytosis as well as ROS can drive macrophage polarization towards the M2 state, meaning that ROS not only has phagocytic but also signaling function [16][17]. Not only is ROS required for M2 polarization, but in this state the cells generally have lower levels of ROS due to diminished ROS producing enzymes in addition to higher amounts of antioxidant enzymes, such as GPX1, [11] while also being phagocytically less active [18].

Understanding this close relationship between macrophages and ROS, especially how oxidative stress affects the metabolism of macrophages, may act as a way to gain insight into the molecular workings of macrophages. Grasping the underlying mechanisms of macrophage functions is important, because these cells contribute to inflammatory diseases, notably cancer [6].

1.2 Role of Macrophages in Cancer

Cancer proves to be a major problem to public health with ever increasing incidence [19]. Due to the vast amount of oncogenic alterations the heterogeneity of tumors means complexity in trying to effectively target it. Cancer may be driven by increased cell proliferation, resistance to cell death, no replicative limit, an increase in mutations, and immune evasion strategies among many other factors [20]. There have been many different forms of cancer treatments over the last decades [21]. Yet due

to the complexity and heterogeneity of this ailment further progress towards effective treatments is desirable.

The first cancer therapies consisted of surgical removal of tumors, using radiation to damage cancer cells or deploying chemicals lethal to highly replicative cells. Yet due to applicatory limitations and severe side effects other medical practices have been developed such as hormonal based treatments among others. Current research concerns itself with alternative methods such as immunotherapy [21] or treatments addressing the tumor micro environment (TME) [22]. Macrophages may be a site of interest for both of these treatment options due to on the one hand being able to combat cancer as M1-like macrophages but on the other hand also having a supporting role in the TME as M2-like macrophages [23]. The antitumor properties of macrophages stem from the ability to kill cancer cells through phagocytosis [18] as well as having other mechanisms to destroy tumors in the M1 polarization state that aren't fully elucidated yet [24]. M1 macrophages are also associated with better cancer patient survival, through recruitment of T and NK cells to the TME, that secrete cytokines that activate antitumorigenic pathways [23]. On the other hand macrophages that are found in the TME, also known as tumor associated macrophages (TAMs), represent the M2 phenotype and are able to support tumor progression through angiogenisis, providing growth factors, suppressing immune response, aiding cell proliferation and other mechanisms [23][6]. Tumors even have the ability to hijack macrophages and shift polarization from the anti-tumor M1 state towards the M2 phenotype [23].

Since a current site of interest for targeted cancer therapies is the TME [22], with macrophages being abundant there, they might act as an important key player in future tumor treatments [18], for instance, by promoting M1 polarization of naive macrophages to utilize their phagocytic capabilities to kill cancer cells in immunotherapy, inhibiting the protumor properties of M2-like macrophages, or converting the M2 polarized TAMs to the M1-like phenotype. By understanding the signatures and mechanisms of macrophage polarization on a subcellular level, methods can be developed to benefit from this phenomenom for future cancer treatments. Yet it has also been reported that the cytotoxicity of M1 macrophages might drive tumors towards being more aggressive and evading the immune system [25], so it is even more of importance to elucidate the nuances of macrophage polarization.

1.3 Hallmarks of Macrophage Polarization

In cell models naive human monocyte-derived macrophages (M0 state) and macrophages with the M1-like phenotype or the M2-like phenotype are available [26]. The suspension cell line U937 of pro-monocytic cells [27] can be differentiated into M0 macrophages using phorbol 12-myristate 13-acetate (PMA). These naive macrophages can be further polarized into M1-like macrophages using LPS or into M2-like macrophages using macrophage colony-stimulating factor (M-CSF) and subsequent interleukin-4 (IL-4) treatment [28]. Originally the classification was based on the underlying Th1 or Th2 responses resulting in macrophages either producing pro- or anti-inflammatory cytokines and fulfilling different immune functions [29]. Not only can these polarization types be distinguished by their biological function, but also on molecular level by proteomic and metabolomic signatures. One of the first metabolic differences discovered between M1 and M2 macrophages was their arginine metabolism. In the pro-inflammatory state macrophages breakdown arginine to nitric oxide (NO), which has antipathogenic properties, using nitric oxide synthase (NOS), whereas the anti-inflammatory M2 macrophages metabolize arginine to ornithine and urea using arginase (ARG1), which leads to the production of trophic polyamines [30][29]. Energetically the cells differ from another by the fact that M1 macrophages rely on glycolysis for ATP production, while M2 macrophages primarily use

oxidative phosphorylation (OXPHOS). The reason for this is the hypoxic environment in inflamed tissues leading to cells relying more on glycolysis for their energy household as a precaution against damaged mitochondria and reduced respiratory capabilities due to high levels of ROS produced by the cells or present in the tissue [31][10]. On the other hand, intermediates of glycolysis can be fueled into the pentose phosphate pathway resulting in the production of ROS generating NADPH oxidases [32]. The enhanced glycolytic activity of M1 macrophages leads to a reconstructed citric acid cycle, which in turn leads to accumulation of itaconate and succinate, which represents a metabolic signature for the pro-inflammatory polarization state [33]. In contrast to this, M2 macrophages meet their metabolic demands through glutaminolysis, which leads to the accumulation of α-ketoglutarate that is needed for OXPHOS and fatty acid oxidation. Therefore, α-ketoglutarate represents a metabolic hallmark for M2 polarization [32][33]. Their lipid metabolism also differs fundamentally. M1-like cells rely on the biosynthesis of fatty acids which are used as precursors for inflammatory signaling molecules, whereas M2 macrophages oxidize fatty acids to fuel their energy cycle [34].

Yet macrophage polarization is a dynamic process in which the M1 and M2 states merely represent two extremes at either end of a gradient with the cells' functionality being able to move along this gradient and switch between states (see figure 1). This also means that the polarization state of macrophages can lie between the M1 and M2 phenotype leading to macrophages presenting a hybrid of pro- and anti-inflammatory properties [23]. The plasticity of macrophage polarization leaves room for further elucidation of the hallmarks and mechanisms that underlie this biological process. This may be achieved using mass spectrometry (MS) coupled with liquid chromatography (LC). LC-MS is an analytical technique that can generate both structural and quantitative data of molecules while being very sensitive, therefore it is used as a detection method for analytes of interest. It is commonly used to detect cellular components, such as proteins as well as metabolites, making it an important tool in proteomics and metabolomics analysis [35].

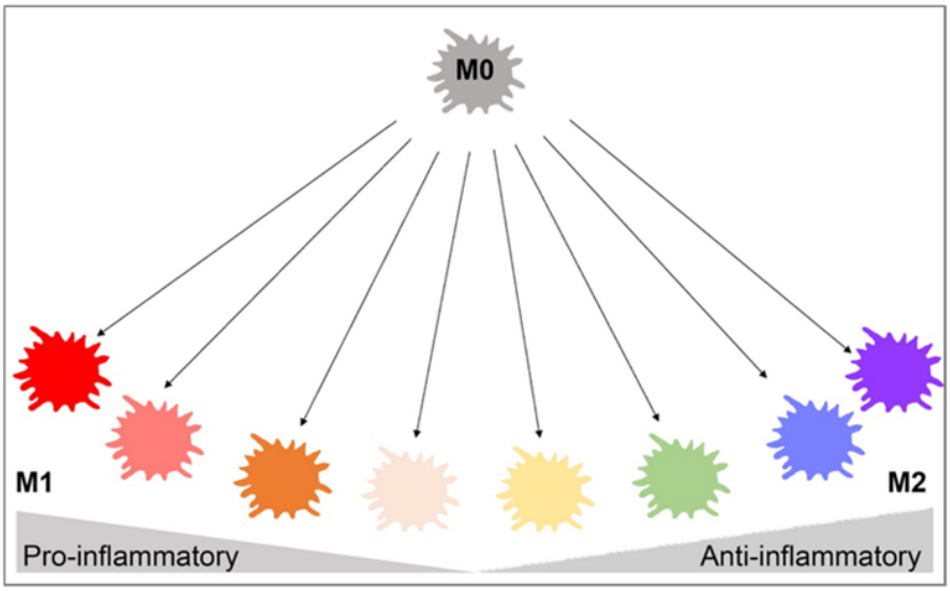

Figure 1: Macrophage polarization depicted as a gradient, where the M1 and M2 states act as extremes on either ends allowing for a plethora of mixed functional states between the two. This figure was reprinted with permission from [23]

1.4 Liquid Chromatography-Mass Spectrometry

To analyze proteins or metabolites from a complex mixture, the first step generally consists in separating the analytes using liquid chromatography [35]. Separation is achieved through varying interactions of the analytes with the mobile and stationary phase. A common chromatographic technique is reversed-phase LC (RPLC), which utilizes a polar mobile phase and a hydrophobic stationary phase. Molecules interact with the stationary phase based on their hydrophobicity, and are eluted using a gradient starting with water then increasing the organic solvent content in the mobile phase, resulting in hydrophilic analytes eluting first followed by analytes with increasing hydrophobicity [36][37]. This separation technique can be used for peptides and proteins but when analyzing the metabolome, which contains in addition to apolar also polar and charged molecules, such as phosphates as well as carboxylic acids, other chromatographic methods must be used. One possibility is to utilize ion-pairing (IP) chromatography, which provides an additional retention mode to common RPLC by adding an ion-pairing reagent, which is an amphiphilic molecule, to the mobile phase. This reagent, such as tributylamine, which has a positively charged moeity as well as hydrophobic rests, can form an ion-pair with polar and negatively charged analytes, which can then be retained in the apolar stationary phase [36].

This separation technique can then be coupled with a mass spectrometer, which allows ionized molecules in the gas phase to be further separated and analyzed qualitatively based on retention times, mass to charge ratios m/z and specific fragmentation spectra, or quantitatively based on peak intensities. A mass spectrometer consists of ion source, mass analyzer and detector. After separation in the liquid chromatography system the charged analytes are brought into the gas phase using an ion source, that utilizes for instance electrospray ionization (ESI). Using this heated source, analytes dissolved in a volatile solvent are nebulized to small droplets by a jet with an applied electrical current which leads to ionization of the analytes through redox reactions. The charged droplets are further evaporated until they reach their Rayleigh limit. The internal Coulomb repulsion leads to bursting of the particles, called Coulomb-explosion, which leaves behind the ionized analyte in the gas phase. Analyzation of the ions can be conducted through different methods, for instance, using time-of-flight (TOF) instruments, which characterize analytes based on the time spent during flight in a field-free space, which is m/z dependent. Another common instrumentation technique for ion analysis is the quadrupole. This consists of cylindrical electrodes which apply alternating electrical fields that allow ions with certain m/z to pass through and be detected. To get additional qualitative information, ions are further fragmented in a collision cell. The obtained fragments are also detected and specific fragment patterns give supplementary qualitative information on the ions. Detection in its simplest form is an electrical signal generated when an ion transfers its charge to an electrode [38].

To analyze the proteins of cells, an untargeted method using trapped ion mobility spectrometry (TIMS) coupled with TOF-mass spectrometry was chosen. In usual data dependent analysis precursor ions are fragmented selectively, whereas others that might elute at the same time are discarded. Using TIMS multiple simultaneously eluted precursors can be trapped and separated based on their ion-mobility. In the following TOF-MS each ion can be qualified with higher selectivity [39].

To gain insight into the metabolome of cells, a targeted approach based on triple quadrupole (QQQ) mass spectrometry was used. A method chosen for the quantification of 193 metabolites using QQQ MS was multiple reaction monitoring (MRM). In the first quadrupole (Q1) a precursor ion is selected based on its specific m/z. This ion is passed into the second quadrupole (Q2) which acts as a collision cell where the precursor is fragmented. In the last quadrupole (Q3) specific products are transmitted

for detection and quantification. This combinatory method allows for sensitive measurement of specific target analytes. Monitoring the analytes only in a time window when they are expected allows for dynamic building of MRM transition lists (dMRM) [40].

2 Aim of the Work

This thesis aims to elucidate metabolic differences between differently polarized macrophages and what role oxidative stress plays in macrophage polarization. To achieve this, U937 cells were differentiated into M0-, M1- and M2-like macrophages in cell culture experiments while being treated with and without an oxidant, tert-butyl hydroperoxide (TBHP). Control U937 cells were treated the same. After extracting the metabolites of whole cell lysates (WCL) and supernatants (SN), those were measured on an ion-pairing LC-MS system to determine the macrophage functionality at metabolomic level as well as how oxidative stress plays into this. In parallel to this a different cell experiment was ran where the same cell groups were left untreated to conduct proteomics analysis using LC-MS in order to confirm successful macrophage polarization into the intended states and correlate some of the results of the metabolomics analysis with changes at protein level. Additionally, MTT assays using TBHP and tests to determine the exact cell count after TBHP treatment of U937 cells and M0-like macrophages were done to establish a concentration to use before differentiation of U937 cells in the metabolomics experiment. The importance of this work lies in the fact that understanding the mechanisms of macrophage polarization is important for building the big picture of cancer progression and can be utilized to develop novel anti-tumor therapies.

3 Materials and Methods

3.1 Materials and Devices

Table 1: Materials used

1,4-Dithio-D,L-threitol (DTT)	GERBU Biotechnik
2-Chloracetamide (2-CAM)	Sigma-Aldrich
3-[(3-Cholamido-propyl)-dimethylamino]	GERBU Biotechnik
-1-propane-sulfonate (CHAPS)	
6-Well plate	Sarstedt
96-Well plate	Sarstedt
Acetic acid, 100%	Sigma-Aldrich
Acetonitrile (ACN)	Honeywell, Riedel-de-Haen
N-Acetylserotonin-d3	BIOZOL Diagnostica
Albumin Fraction V (BSA)	Carl ROTH
Ammonium hydroxide (NH_4OH) 28% in water	Sigma-Aldrich
tert-Butyl hydroperoxide solution (70 wt. % in H_2O)	Sigma-Aldrich
Cell culture flask, T-75, suspension, filter cap	Sarstedt
Conical centrifuge tubes (15 ml)	Falcon, Corning
Dimethyl sulfoxide (DMSO), dried	Sigma-Aldrich
Empore^{TM} C18 Solid Phase Extraction Disk	CDS Analytical
Empore^{TM} SDB-PRS Solid Phase Extraction Disk	CDS Analytical
Fetal Bovine Serum (FBS)	Gibco
Formic acid	Sigma-Aldrich
Hydrochloric acid fuming 37% (HCl)	Merck
Isopropanol (IPA)	Sigma-Aldrich
α-Ketoglutaric acid-C13	Sigma-Aldrich
Lipopolysaccharides from E. coli (LPS)	Sigma-Aldrich
Methanol (MeOH)	Honeywell, Riedel-de-Haen
Penicillin-Streptomycin	Sigma-Aldrich
Trypan Blue Solution (0.4%)	Sigma-Aldrich
Phorbol 12-myristate 13-acetate (PMA)	Sigma-Aldrich
Protein Assay Dye Reagent Concentrate (Bradford reagent)	Bio-Rad
Recombinant Human Interleukin-4 (IL-4)	ImmunoTools
Recombinant Human Macrophage	ImmunoTools
colony-stimulating facor (M-CSF)	
RPMI-1640 Medium	Sigma-Aldrich
Safe-Lock Microtubes (1.5/2 ml)	Eppendorf
Sodium deoxycholate (SDC)	Sigma-Aldrich
Sodium dodecylsulfate (SDS)	GERBU
Sodium pyruvate (100 mM)	Gibco
Standard peptide mix	Peptide Specialty Laboratories
Succinic acid-d4	Sigma-Adlrich
Thiazolyl Blue Tetrazolium Bromide (MTT)	Sigma-Aldrich

Table 1 Continued

Thiourea	Sigma-Aldrich
Tributylamine (TBA), 99%	Acros Organics
Trifluoracetic acid (TFA)	Sigma-Aldrich
Tris (2-carboxyethyl) phosphine (TCEP), Bond-Breaker^{TM} TCEP solution, pH 7, 500 mM	Thermo Fisher Scientific
Tris-(hydroxymethyl)-aminomethane (TRIS)	GERBU Biotechnik
Trypsin/EDTA (0.05%/0.02% in DPBS)	PAN-Biotech
Trypsin/Lys-C Mix	Promega
U937 cells	ATCC
Urea	Fluka
Water (H_2O)	VWR Chemicals

Table 2: Devices used

Cell counter	CellDrop BF (DeNovix)
Centrifuge	accuSpin Micro 17 (Thermo Fisher Scientific)
Centrifuge	Centrifuge 5425 R (Eppendorf)
Centrifuge	Heraeus Megafuge 16R (Thermo Fisher Scientific)
HPLC system	1290 Infinity II (Agilent)
Incubator	Heracell 150i (Thermo Fisher Scientific)
Mass spectrometer	6490 Triple Quad LC/MS (Agilent)
Mass spectrometer	timsTOF Pro (Bruker)
Microscope	AxioCam ERc5s (Zeiss)
Photometer	Multiskan GO (Thermo Fisher Scientific)
Thermoshaker	ThermoMixer C (Eppendorf)
Thermoshaker	Thermomixer comfort (Eppendorf)
UHPLC system	Dionex UltiMate^{TM} 300 RSLCnano (Thermo Fisher Scientific)
Ultrasonicator	S220 Focus-ultrasonicator (Covaris)
Ultrasonic bath	Sonorex Digital 10P (Bandelin)
Speedvac	miVac DUO concentrator (Genevac)

3.2 Cell Culture

3.2.1 General Procedures

U937 cell line was cultured in RPMI-1640 medium supplemented with 1% Penicillin-Streptomycin, 10% Fetal Bovine Serum and 1% 100 mM Sodium pyruvate solution in suspension T-75 cell culture flasks with vented caps at 37 °C and 5% CO_2. The cells were subcultured by discarding a certain amount of cell suspension and replacing with fresh medium to achieve the desired split ratio. Cells were pelleted by transferring the suspension to a 15 ml centrifuge tube (Falcon) and centrifugation at 172 ×g and 23 °C for 5 min (Heraeus Megafuge 16R) before removing the used medium. To count the cells the pellet was resuspended in 1 ml of medium, then 10 µl were added to 90 µl of PBS and mixed with 100 µl of Trypan Blue, 10 µl of the resulting mixture were pipetted onto the clean sample slide of the Brightfield cell counter. A dedicated counting method for the U937 cell-line was used to determine the live, dead and total cell count.

Table 3: Composition of PBS buffer pH = 7.4

Compound	Concetration [mM]
NaCl	137
KCl	2.7
Na_2HPO_4	10
KH_2PO_4	1.8
Water	-

3.2.2 MTT Assay

MTT assays can be used to determine the concentration of a compound at which cells stop being metabolically active, by letting the cells metabolize MTT to formazan crystals after treatment. These assays were conducted to determine the viability of U937 cells and M0-like macrophages put under oxidative stress using TBHP. The colorimetric assays were carried out in 96-well plates with a border of 100 µl PBS in the outer wells. U937 cells were seeded in the plates by pipetting 75 µl of medium containing 10,000 cells in 3 × 9 wells. M0-like macrophages were seeded by adding 75 µl of medium with 100 ng/ml PMA containing 10,000 U937 cells in 3 × 9 wells, the cells were then allowed to differentiate by 72 h incubation. For the blank 3 wells were filled with 75 µl of medium. After seeding the cells were treated for 24 h with TBHP by adding column-wise 25 µl of medium containing different concentrations of TBHP. The TBHP amount for the U937 cells as well as for the differentiated U937 cells ranged from 0 to 500 µM, each in replicates of 3. After 24 h incubation 10 µl of a 5 mg/ml MTT solution in PBS was added to each well and the plates were incubated for another 4 h. To dissolve the formazan crystals the medium was carefully removed and 100 µl of DMSO was added to the wells, for the suspension U937 cells an extra centrifugation step at 172 ×g for 5 min (Heraeus Megafuge 16R) was done before medium removal. The plates were shaken lightly, then the absorbance of each well was measured in the photometer at 570 nm. Using GraphPad Prism (version 6.07) dose-dependence curves and the IC50 values of TBHP can be calculated and visualized by plotting the mean of 3 wells against the logarithm of the concentration of TBHP of said wells.

3.2.3 Cell Counting Test

In addition to the MTT assays a series of tests were done to determine how TBHP treatment effects the amount of U937 cells that die as well as the amount that differentiate with subsequent PMA treatment. This was done using Trypan Blue cell counting. U937 cells were seeded at a density of $1*10^6$ cells in 3 ml of medium in a six well plate. In a separate plate they were seeded with an additional 60 µM of TBHP. After 1 h incubation 10 µl of a 30 ng/µl PMA solution in medium was added to 3 wells of each plate resulting in 100 ng/ml PMA to achieve U937 differentiation. After 24 h incubation the floating and adherent cells were counted. To count the floating cells 50 µl of medium from the wells was mixed with 50 µl of Trypan Blue and 10 µl of this mixture was pipetted into the cell counter. To count the adherent cells the supernatant was completely removed and the wells were washed with 1 ml of PBS. 300 µl of Trypsin/EDTA (0.05%) was added to each well and the plates were incubated for 7 min at room temperature (RT). Afterwards 2.5 ml of medium was added to the wells to stop the reaction and the cell suspensions were transferred to 15 ml centrifuge tubes (Falcon). The cells of each well were pelleted and resuspended in 1 ml of medium, 50 µl of cells were mixed with 50 µl of Trypan Blue and 10 µl of this mixture was pipetted on the cell counter sample arm to count the cells. This test was done twice as well as repeated with $2*10^6$ cells treated with 60 or 80 µM

TBHP. Additionally, another test using only U937 cells differentiated with PMA for 48 h after being treated with and without 100 µM TBHP was conducted.

3.2.4 U937 Differentiation

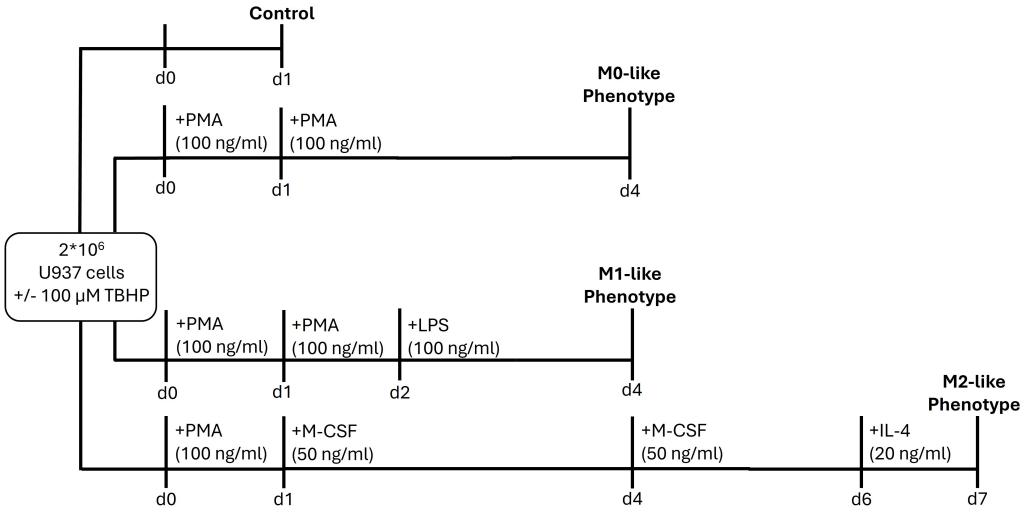

Figure 2: Timeline for U937 differentiation into M0-, M1- and M2-like macrophages as well as control U937 cells. Each path seeded with $2*10^6$ cells and treated with or without 100 µM TBHP in six replicates

U937 differentiation was conducted according to the timesheme shown in figure 2. To start the differentiation of U937 into different macrophage phenotypes, $2*10^6$ cells in 3 ml of medium containing 100 ng/ml PMA were seeded into each well of a 6-well plate, one plate per phenotype. Additionally, to see the effects of ROS on macrophage polarization, each differentiation path was repeated with 100 µM of TBHP in the medium during cell seeding. After 24 h the medium was changed for all plates while keeping the undifferentiated cells by carefully removing the used medium from the wells then pelleting the floating cells which were then resuspended in fresh medium containing 100 ng/ml PMA for M0- and M1-like macrophages and 50 ng/ml M-CSF for the M2-like phenotype. The cells in 3 ml of fresh medium were then added back to the respective wells. After a subsequent 72 h incubation the M0-like macrophages were retrieved. For the M1-like phenotype after another 24 h incubation step 100 ng/ml of LPS was added to the cells in fresh medium, after 48 h the U937 cells were polarized into M1-like macrophages. To achieve M2-like polarization after 72 h another 50 ng/ml M-CSF in fresh medium was added to the cells followed by a medium change containing 20 ng/ml IL-4 after 48 h, incubation for 24 h lead to M2-like macrophages. In addition to this, a set of control U937 cells (CON) were seeded at $2*10^6$ cells in 3 ml in 6-well plates with and without 100 µM of TBHP then incubated for 24 h.

3.3 Proteomics

The cells used for this experiment were differentiated according to figure 2 without TBHP and only in three instead of six wells each. Additionally, the control cells were harvested on d0 directly from the culturing flask. The U937 cells were analyzed looking at their proteomic profiles to determine whether the polarization according to figure 2 was successful.

3.3.1 Whole Cell Lysis

Table 4: Composition of SDC lysis buffer

Compound	Concentration [mM]	Percentage (% wt/vol)
SDC	-	4
TRIS-HCl 2M pH 8.5	100	-
Water	-	-

Harvesting of cells was conducted over ice, with cold solutions and with a centrifuge (Heraeus Megafuge R16) cooled to 4 °C. Lysis of control U937 cells was done by pelleting, resuspending in 1 ml then counting cells of a TC flask. From the cell pellet 300 µl containing $3*10^6$ cells was taken and washed 3x with 1 ml of PBS in a 1.5 ml microtube (Eppendorf) by centrifuging the tube for 5 min at 161 ×g then removing the PBS completely from the cell pellet. To the cells 390 µl of SDC lysis buffer was added and the tube was heated to 95 °C in a thermoshaker for 5 min. The lysed cells were divided into 3 aliquots of 130 µl containing $1*10^6$ cells each. Differentiated U937 cells were harvested by carefully removing the medium in the wells then washing the adherent cells twice with 1 ml of PBS. To each well 130 µl of SDC buffer was added and the cells were scraped from the well surface then transferred to 1.5 ml microtubes (Eppendorf). The tubes were heated in a thermoshaker at 95 °C for 5 min.

To homogenize the WCL the ultrasonicator (Covaris) was used. The microcapsules were prepared with two teflon bars and filled with 130 µl of sample, then secured in a ultrasonication chamber to be placed in the water bath. Cell homogenization was achieved by running a method with 190 W peak incident power, 20% duty factor, 200 cycles per burst at 15 °C for 2 min. The whole cell lysates were stored at -20 °C until further use.

3.3.2 Protein Quantification via BCA Assay

To determine the protein concentration of the U937 differentiation samples a BCA assay was performed. For this colorimetric assay a BSA calibration curve ranging from 0-9 µg/µl was prepared on a 96-well plate, by mixing the appropiate amount of a 1 µg/µl BSA solution in water into 1 µl of SDC buffer and water to the total volume of 10 µl. On the same microtiter plate 1 µl of WCL sample was added to a well with 9 µl of water. To each well 200 µl of working reagent was added, which consists of a 50:1 ratio mixture of BCA reagent A (see table 5 for composition) and BCA reagent B, which is a 200 mM $CuSO_4 \cdot 5H_2O$ solution in water. The plate was placed in a plate shaker for 1-2 min at 1100 rpm then incubated at 60 °C for 30 min. Afterwards the absorbance of each well was measured in the plate reader at 562 nm.

Table 5: Composition of BCA reagent A pH 11.25

Compound	Concentration [mM]
Bicinchoninic acid	29.0
Sodium carbonate	188.7
Sodium tartrate	8.2
Sodium bicarbonate	113.1
Water	-

3.3.3 Protein Digestion

To prepare the proteins for MS measurement an in-solution digestion was performed. Using the results from the BCA assay the amount of each sample containing 20 µg of protein was calculated. The volume was then filled to 90 µl with SDC buffer. To each sample 2 µl of 500 mM TCEP pH 7 solution was added to reduce the disulfide brigdes in proteins. The samples were vortexed then incubated for 5 min at 45 °C and 1200 rpm in the thermoshaker. To alkylate the proteins 5 µl of an aqueous 800 mM 2-CAM solution was added to each sample, which were then vortexed and incubated in the thermoshaker for 5 min at 45 °C and 1200 rpm. A cold 0.1 µg/µl Trypsin/LysC solution was prepared by dissolving 20 µg of enzyme with 200 µl of 50 mM acetic acid. Working on ice, 2 µl of the prepared enzyme solution was added to each cooled sample, which were then vortexed and incubated in the thermoshaker at 37 °C and 1200 rpm for 5 h. Afterward another 2 µl of cold enzyme solution was added to the cooled samples, which were then vortexed and incubated in the thermoshaker for 15 h at 37 °C and 1200 rpm for successful protein digestion.

3.3.4 SDB-PRS StageTip Cleanup of In-Solution Digests

To clean the proteomics samples before MS analysis a StageTip cleanup, using 200 µl pipette tips stuffed with 3 layers of SDB-PRS solid phase extraction (SPE) material, was performed. To condition the StageTips they were placed in 2 ml microtubes (Eppendorf) and 150 µl of loading buffer (1% TFA in IPA) was pipetted onto the SPE material. The tips were then centrifuged for 3 min at 1000 ×g until the loading buffer was 1 mm above the extraction material. The samples after protein digestion (see above) were reduced to 30 µl by drying in the speedvac for 35 min at 45 °C then let cool to room temperature. The samples were then dissolved in 120 µl of loading buffer through vortexing, using the ultrasonic bath then pipetting up and down. The samples were then transferred each to a conditioned StageTip and the old tube (Eppendorf) was washed using 50 µl of loading buffer which was then transferred to the respective StageTip. To bind the proteins to the extraction material, the tips were centrifuged for 5 min at 500 ×g until all buffer passed through then the waste tubes were emptied out. The tips were washed by adding 100 µl of loading buffer and then centrifuging for 2 min at 1500 ×g until everything passed through, with the wash being discarded afterward. Another washing step was performed by adding 100 µl of wash buffer (5% ACN, 0.2% TFA in water) to the tip and pipetting up and down inside the tip to dissolve any remaining pellets. The StageTips were then centrifuged for 1 min at 1000 ×g. The tips were then places in glass inserts inside new microtubes (Eppendorf), 30 µl of elution buffer (60% ACN, 0.0014% NH_4OH in water) was pipetted on top of the SPE material and the tips were centrifuged for 1 min at 300 ×g until everything passed through. Another 30 µl of elution buffer was added and the tips were centrifuged for 8 min at 1500 ×g until all went through. The eluted samples were dried in the speedvac for 1 h at 45 °C.

3.3.5 Peptide LC-MS/MS Analysis

To measure the peptides gained by in-solution digestion of proteins and subsequent StageTip cleanup (see above) they were first reconstituted by adding 400 µl of water to the 2 ml storage tube containing the sample in a glass insert. To the dried sample 5 µl of 10 fmol standard peptide mix (see Appendix table 10 for composition) in 30% formic acid was added and mixed to dissolve the peptides. To the insert 40 µl of MS loading buffer (0.05% TFA, 2% ACN in water) was added and the sample was mixed. The glass insert was placed in the water in the storage tube and the samples were sonicated in

the ultrasonic bath for 5 min at 40% power. The samples were spun down for 7 min at 5000 ×g before transferring the inserts to MS vials, which were then placed in the autosampler of the LC system.

Chromatographic separation of the peptides was achieved on a Dionex UltiMate^{TM} 300 RSLCnano system. A volume of 5 µl of reconstituted peptides was loaded onto the Acclaim PepMap^{TM} C18 100 (Thermo Fisher Scientific) pre-column using solvent A (0.1% formic acid in water) at a flow rate of 10 µl/min. The peptides were eluted onto the Aurora series emitter, 1.6 µm C18, 25 cm · 75 µm (IonOpticks) analytical column and the analytes were separated using a gradient ranging from 12% to 42% of solvent B (79.9% ACN, 20% water, 0.1% formic acid) over a period of 90 min at a flow of 300 nl/min. Inlcuding column equilibration and wash the total run time of the method per sample was 140 min.

The MS/MS measurements of the proteomics samples was performed on the timsTOF Pro mass spectrometer (Bruker). The MS1 and MS2 spectra analysis was achieved in parallel accumulatiom-serial fragmentation (PASEF) and data dependent acquisition (DDA) mode, with a m/z range from 100 to 1700. To separate the analytes based on trapped ion mobility an inverse ion mobility (1/k0) scan ranging from 0.6 to 1.6 Vs · cm^2 totaling to 100 ms of ramp time was used. For 10 PASEF MS/MS scans the total cycle time took 1.16 s.

3.3.6 Data Processing

The acquired LC-MS data was processed using MaxQuant v 1.6.17.0 with the Andromeda search engine [41]. Label-free quantification (LFQ) and identification of proteins was achieved by searching against the SwissProt "*homo sapiens*" database (vesrion 141219 with 20380 entries) with a peptide mass tolerance of 40 ppm and maximal two missed cleavages. Carbamidomethylation was a fixed modification while methionine oxidation as well as N-terminal protein acetylation were set as variable modifications. For positive identification at least two peptides, one of them unique, were required and the "match between runs" setting was enabled with a match time window of 0.7 min, an alignment time window of 20 min, a match ion mobility window of 0.05 as well as an alignment ion mobility of 1. A false discovery rate ≤ 0.01 was set for peptide and protein identification by computing a reverse decoy database.

For subsequent data analysis and evaluation Perseus (version 1.6.14.0) was used with reverse sequence and common contaminant filtering [42]. LFQ intensity values were $\log_2$-transformed and proteins were filtered for a minimal number of 5 out of 6 independent identifications in at least one group. Imputation of missing values was done from normal distribution with a width of 0.3 and a down shift of 1.8. The statistical analysis as well as data visualization were also done in Perseus (version 1.6.14.0). To determine proteins significantly regulated between different macrophage types, two-sided t-tests employing multiparameter correction with a q-value 0.01 were applied.

3.4 Metabolomics

The differentiated U937 cells as well as the control cells treated with and without TBHP according to figure 2 were used for the following described metabolomics analysis.

3.4.1 Metabolite Extraction from WCL and SN

The extraction process was conducted over ice and with a centrifuge (Heraeus Megafuge 16R) cooled to 4 °C on the last day of each respective differentiation schedule (figure 2). Harvesting whole cell

lysates (WCL) was done by transferring the cell suspension from the wells to 15 ml polypropylene tubes (Falcon), pelleting the floating cells (CON +/-TBHP) then dissolving them in 500 µl of extraction buffer which was then divided into 3 aliquots of 150 µl into 1.5 ml safe-lock microtubes (Eppendorf). For the adherent cells the supernatant was removed completely from the wells and the cells were scraped from the wells in 500 µl of extraction buffer, which was then divided into 3 aliquots of 150 µl. The metabolites in the supernatants (SN) were extracted by collecting 100 µl from the top after centrifugation, 5 min at 172 ×g, which was then mixed with 400 µl of extraction buffer before being aliquoted into 3x 150 µl. Additionally, the medium control was obtained by letting 3 ml of medium in each well of a 6-well plate incubate for 24 h before taking 100 µl from each well and mixing it with 400 µl of extraction buffer, which was then divided into 3 aliquots of 150 µl. Each sample was stored at -80 °C. Before each extraction process 10 µl of N-acetylserotonin-d3 (500 ng/µl in H_2O) was added to each well and mixed in by shaking the plate lightly. Furthermore, the suspensions cells (CON +/-TBHP) were counted before harvesting by taking 50 µl from the homogenised cells suspension of each well and mixing it with 50 µl of Trypan Blue then using 10 µl of this solution to count the cells using the cell counter.

Table 6: Extraction buffers used for extraction of WCL and SN/medium metabolites

Extraction Buffer	Constituents
for WCL	5:3:2 MeOH, ACN, H_2O + 0.4 ng/µl succinic acid-d4
for SN/medium	5:3 MeOH, ACN + 0.5 ng/µl succinic acid-d4

3.4.2 C18 StageTip Filtration

To filter the samples before LC-MS measurement in order to get rid of residual proteins or contaminants for the LC column, 200 µl pipette tips stuffed with 3 layers of C18 (Octadecyl) solid phase extraction material were used. The procedure was done over ice and with the centrifuge (Centrifuge 5425 R) cooled to 4 °C. The samples in 1.5 ml safe-lock microtubes (Eppendorf) were centrifuged at 5000 ×g for 15 min to pellet the proteins. The StageTips were conditioned by adding 100 µl of extration buffer without ISTD (5:3:2 MeOH, ACN, H_2O) to the tips inside 2 ml waste microtubes (Eppendorf) then centrifugation at 500 ×g for 2 min until everything passed through or was slighlty above the C18 material. The tips were then placed on new 2 ml microtubes (Eppendorf). From the samples a volume of 120 µl above the protein pellet was transferred to the conditioned StageTips which were then centrifuged for 2-4 min at 500 ×g. From the collection tube the sample was transferred to a MS vial. The StageTips were rinsed with 50 µl of extraction buffer without ISTD by centrifugation for 2 min at 500 ×g until everything passed through. The wash was then transferred to the respective MS vial. The samples were dried by placing the MS vials under N_2-stream for up to 30 min. The completely dried samples were then stored at -80 °C. This was done for all WCL, SN and medium samples as wells as 6× 1 ml from the pooled SN of CON +/-TBHP.

3.4.3 Protein Quantification via Bradford Assay

Table 7: Composition of sample buffer used in Bradford assay

Compound	Concentration [M]	Percentage (% wt/vol)
Urea	7.5	4
Thiourea	1.5	-
CHAPS detergent	-	4
SDS	-	0.05
DTT	0.1	-
Water	-	-

To determine the total amount of protein in the SN and WCL of all conditions as well as the medium controls, Bradford assays were performed with all samples used for metabolomics analysis. First the protein pelles resulting from the StageTip cleanup of each sample were dried for 20 min the the speedvac at 45 °C. 50 µl of sample buffer (SB) were added to the pellets, which were then placed in the ultrasonic bath for 10 min at 100% sonification. After 15 min heating at 95 °C in the thermoshaker the pellets were sonicated again for 10 min at 100%. A calibration curve of BSA ranging from 0-10 µg/µl was pipetted using a 1 µg/µl BSA solution in water, 1 µl of SB and the volume filled to 200 µl with water in a 96-well plate. The dissolved protein pellets of each sample were pipetted with a volume of 1 µl into 199 µl of water in the same microtiter plate as the respective calibration curve. Then 50 µl of Bradford reagent was mixed into each well before measuring the absorbance of the plate's wells in the photometer at 595 nm.

3.4.4 Ion-pairing LC-QQQ Analysis

Table 8: Composition of solvents for IP QQQ LC-MS

Solvent	Constituents (vol%)
TBA stock	90.2% MeOH, 2.6% anhydrous acetic acid, 7.2% TBA
Eluent A	96.7% H_2O, 3.3% TBA stock
Eluent B	96.7% MeOH, 3.3% TBA stock

To measure the samples prepared as above on an IP triple quadrupol (QQQ) LC-MS system they first were dissolved in 10 µl of eluent B and 90 µl of resuspension buffer (0.5 ng/µl α-ketoglutaric acid-C13 in eluent A). Chromatographic separation of the analytes was achieved on an Agilent 1290 Infinity II high-performance liquid chromatography (HPLC) system. 30 µl of dissolved sample in an insert inside an MS vial were placed in the autosampler of the HPLC system. A volume of 12.5 µl per sample was loaded onto the ZORBAX Extend, 1.8 µm C18, 2.1 x 150 mm, column (Agilent) with 100% eluent A at a flow of 0.25 ml/min. Metabolites were eluted from the column by applying a gradient of 20% to 99% of eluent B between 7.5 min and 24 min of the LC method. Total method time per sample was 40 min including column wash and equilibration.

The MS analysis of the eluted metabolites was performed on an Agilent 6490 Triple Quadrupole LC/MS system. After negative ionization from an ESI source target metabolites were scanned using dynamic MRM. MS parameters were taken from a modified Agilent metabolomics dMRM method (see Appendix table 11).

MassHunter Quantitative Analysis software (Agilent, version 10.1.733.0) was used for data processing and peak integration to obtain the measured analyte responses. Data visualization was performed in Microsoft Excel.

4 Results and Discussion

4.1 MTT Assay

MTT assays were conducted to determine the viability of U937 cells as well as cells differentiated with PMA when exposed to an oxidant and to choose a concentration of TBHP for cell treatment in further experiments.

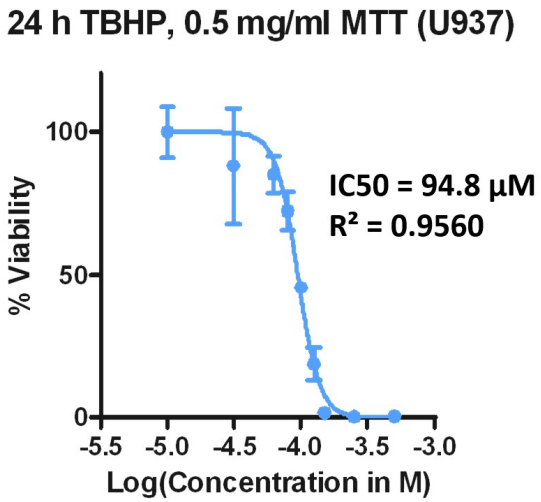

Figure 3: Dose-response curve gained from an MTT assay using U937 cells treated with TBHP for 24 h up to a concentration of 500 µM

When plotting the percentile cell viability, based on the absorbances measured in the wells, against the logarithm of the TBHP concentrations used, it can be seen that this peroxide affects U937 cells in a dose-dependent matter, as can be seen in figure 3. This MTT assay was repeated and from the IC50 values of each dose-response curve the mean was calculated at 92.0 µM for undifferentiated U937 cells (table 9).

Table 9: IC50 values of MTT assays using U937 cells treated with TBHP for 24 h up to a concentration of 500 µM

IC50 [µM]	96.8
	94.8
	87.5
	89.0
Ave	92.0
SD	4.5
rel. SD	4.9%

Yet the dose-response curve of U937 cells first differentiated with PMA for 72 h then treated with TBHP up to 500 µM for 24 h shows a different trend (figure 4).

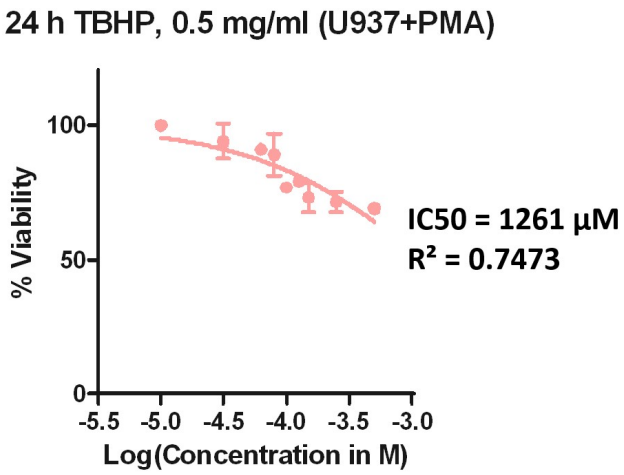

Figure 4: Dose-response curve gained from an MTT assay using U937 cells differentiated for 72 h using 100 ng/ml PMA and subsequently treated with TBHP for 24 h up to a concentration of 500 µM

Looking at figure 4 it can be seen that M0 macrophages don't show the typical dose-dependence when treated with TBHP, instead they have higher viability when put under oxidative stress, hinting towards self-defense mechanisms of this cell type against ROS. In fact macrophages show long survival time in hostile environments *in vivo* due to being equipped with mechanisms that protect them from oxidative damage [9][10].
Due to the missing sigmoidal fit of the dose-response curve, an IC50 value for U937 cells differentiated with PMA could not correctly be calculated. Yet for further experiments the IC50 value of undifferentiated U937 cells is of interest.

4.2 Cell Counting Test

To further investigate the effects of TBHP on U937 viability and differentiation, the amount of cells after peroxide as well as PMA treatment were counted using Trypan Blue staining. This was done to determine the exact amount of cells that were killed when adding TBHP to U937 cells as well as determining the number of cells that differentiated using PMA in combination with peroxide treatment by counting the floating undifferentiated cells and the adherent M0-like macrophages.

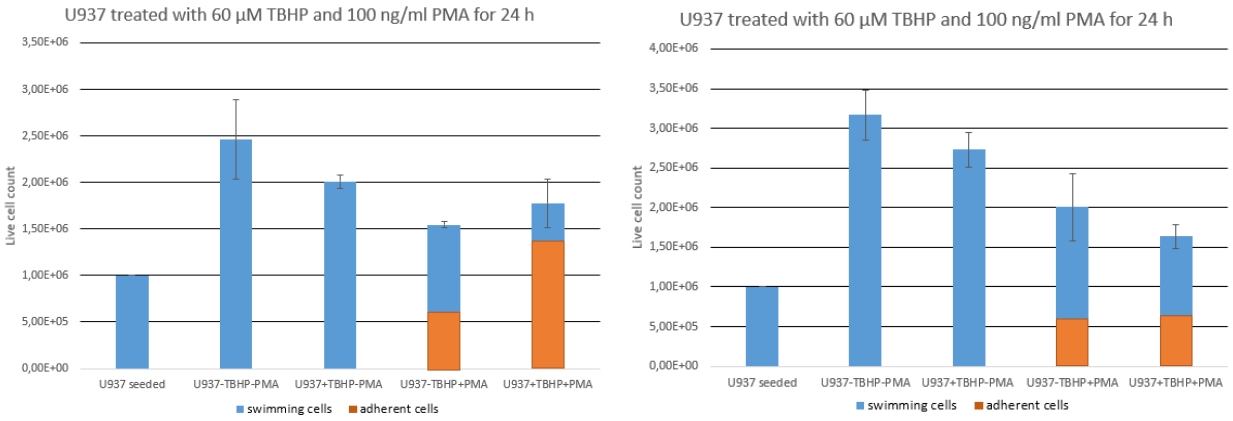

(a) (b)

Figure 5: Two repeats of $1*10^6$ U937 cells treated +/- 60 µM TBHP and differentiated +/- 100 ng/ml PMA and counted after 24 h. The floating and adherent cells were counted for all treatment types

Looking at figure 5a it can be seen that peroxide treatment at a concentration of ca. 60% of the IC50 led to less replicated cells after 24 h. The amount of cells that differentiated using PMA increased from 38% to 76% when combined with TBHP treatment. Yet when repeating this experiment (figure 5b) the amount of differentiated cells increased only from 30% to 37% between the non peroxide and peroxide treated group, only the count of the non-differentiated cells slightly decreased after TBHP addition.

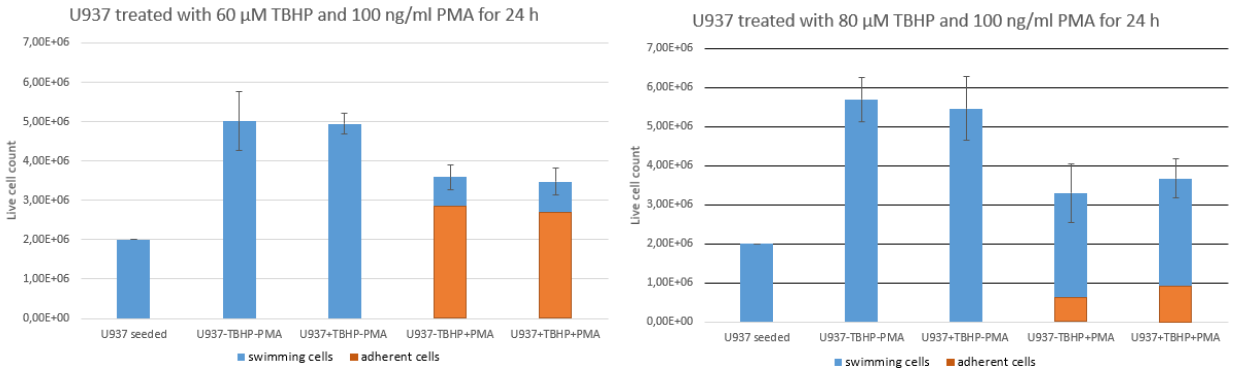

(a) 60 µM TBHP (b) 80 µM TBHP

Figure 6: $2*10^6$ U937 cells treated +/- 60 and 80 µM TBHP then differentiated +/- 100 ng/ml PMA and counted after 24 h. The floating and adherent cells were counted for all treatment types

When $2*10^6$ seeded U937 cells were treated with the same amount of TBHP, differentiation didn't seem to be affected by it, being at 78% for untreated and 76% for TBHP treated cells. But in the control group the relative amount of adherent cells was larger than when starting with $1*10^6$ seeded cells (figure 6a). When treated with 80 µM of TBHP the relative amount of cells that differentiated decreased, with the peroxide treated cells having slightly higher differentiation at 27% compared to 19% (figure 6b).

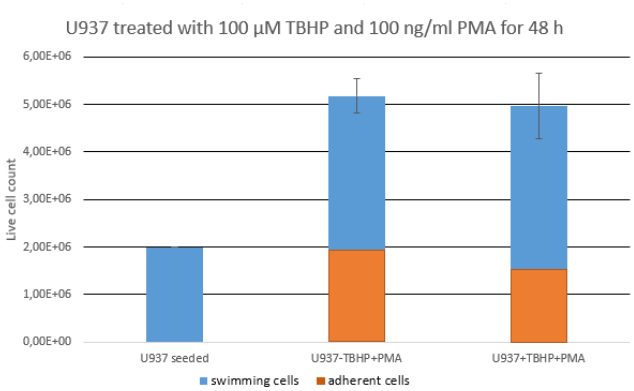

Figure 7: $2*10^6$ U937 cells treated +/- 100 µM TBHP then differentiated with 100 ng/ml PMA and counted after 48 h. The floating and adherent cells were counted for all treatment types

Cells that were seeded at a density of $2*10^6$ cells, treated without and with 100 µM TBHP then differentiated with 100 ng/ml PMA for 48 h replicated to about $5*10^6$ cells (figure 7). This is the same for the non-differentiated U937 cells after 24 h. The TBHP treated cells showed slightly less differentiation at 31% compared to the 37% of the control cells. Interestingly, with TBHP concentration being slightly over the IC50 determined by MTT assays, the live count of the U937 cells barely diminished (figure 7). The same was for $2*10^6$ seeded cells treated with 60 and 80 µM (figure 6). This could be due to the higher cell density allowing the U937 cells to buffer out the peroxide faster leading to increased cell viability even with higher TBHP concentrations. Also ROS are short lived to due their high reactivity [43], which means that after 24 or 48 h the cells have enough time to recover from the oxidative stress. These results also show that MTT assays don't necessarily represent the cell count affected by the TBHP treatment.

Since 100 µM of TBHP in combination with PMA treatment didn't lead to many cells dying, this concentration was chosen to be used when differentiating the cells for metabolomics measurements, since increasing the amount of dead cells would lead to overwhelming amounts of apoptotic signals. Additionally, Kanupriya *et al.* reported that 100 µM of TBHP barely lead to any cell death when investigating the apoptotic effects of TBHP on U937 cells [44].

4.3 Proteomics

Using the obtained proteomic data, macrophage polarization can be highlighted using known protein markers of M1 and M2 macrophages. The presence or absence of proteins as well as the relative abundance between the three replicates of all cell types can be visualized using profile plots. The applied method delivered 5883 identified proteins, with 2231 proteins being significantly regulated in M0 macrophages relative to U937 cells, 242 in M1 macrophages versus M0 macrophages and 1898 in M2 macrophages relative to M0 macrophages. Fewer proteins being significantly regulated between the M1 and M0 macrophages compared to the relation of the other cell types with the M0 macrophages shows the similarity of the M1 and M0 macrophages on a protein level.

A sign that the first differentiation step from monocyte to macrophage worked, is the expression of integrin α-M (ITGAM)(figure 8), which is a cell adhesion molecule causing the differentiated cells to adhere to surfaces [45].

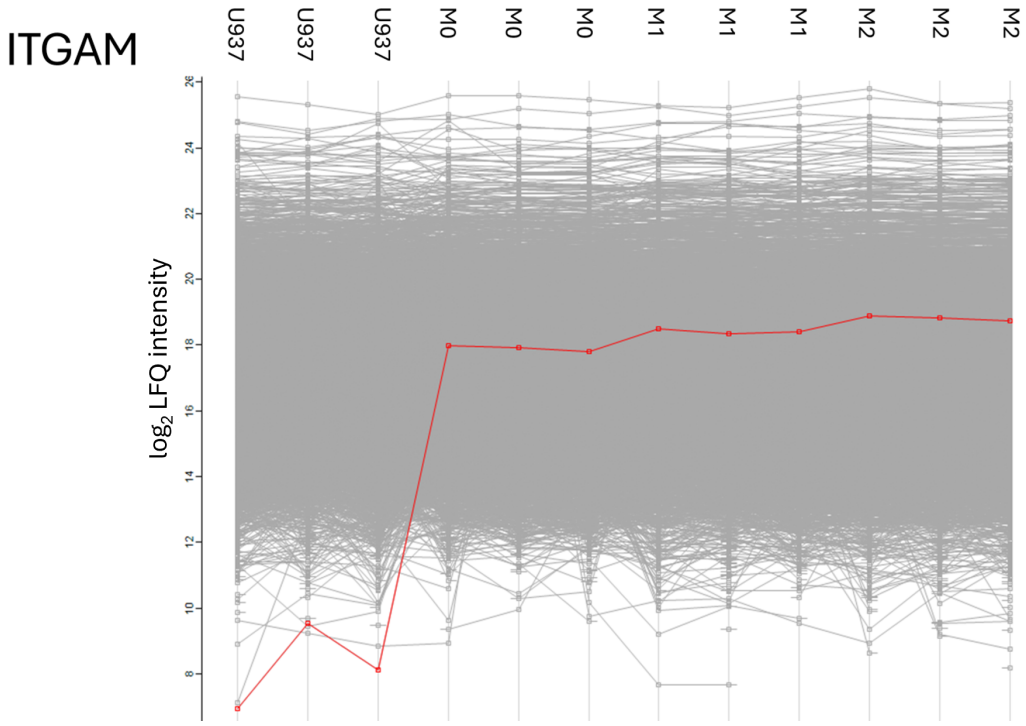

Figure 8: Profile plot of ITGAM $\log_2$ LFQ intensity values of three replicates of each of the U937 differentiation states

4.3.1 Markers for M1-like Macrophages

CD14 is a membrane protein specific for macrophages [28] with higher levels of this protein being expressed by cells of the M1-like phenotype [46].

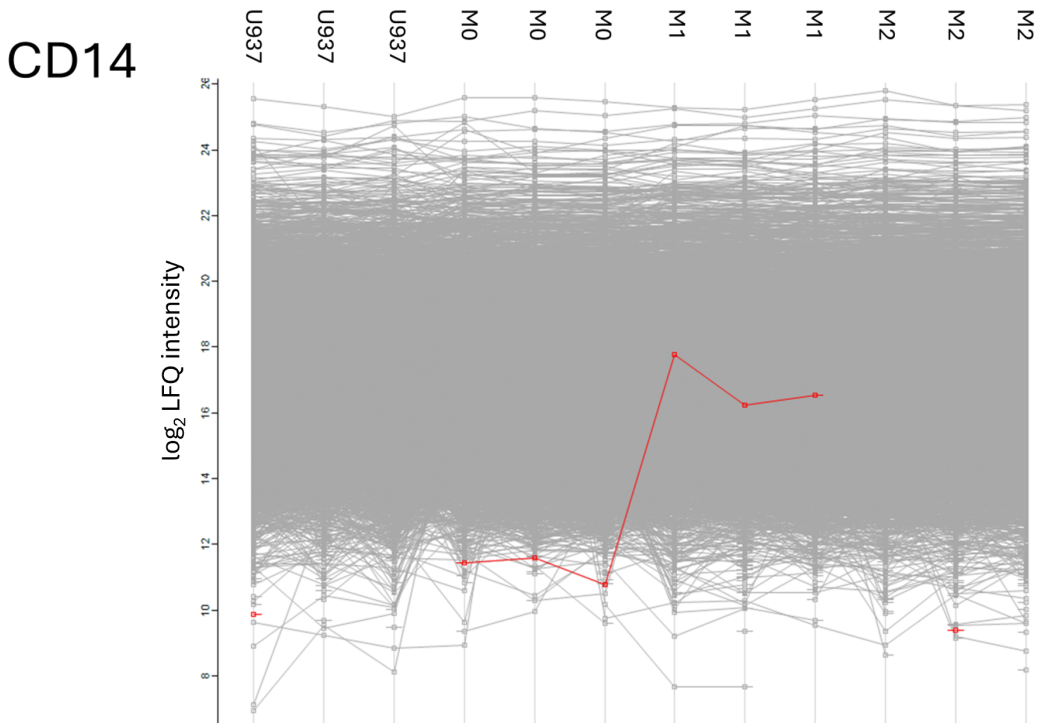

Figure 9: Profile plot of CD14 $\log_2$ LFQ intensity values of three replicates of each of the U937 differentiation states

Looking at the profile plot of CD14 (figure 9), it can be seen that it is only expressed in M0- and

M1-like cells, with levels being significantly higher in the intended M1-like group. Furthermore, as previously mentioned, M1 macrophages produce pro-inflammatory cytokines such as IL-1β [8]. The conducted protocol of macrophage polarization led to the intended M1 macrophages to express IL-1β (figure 10).

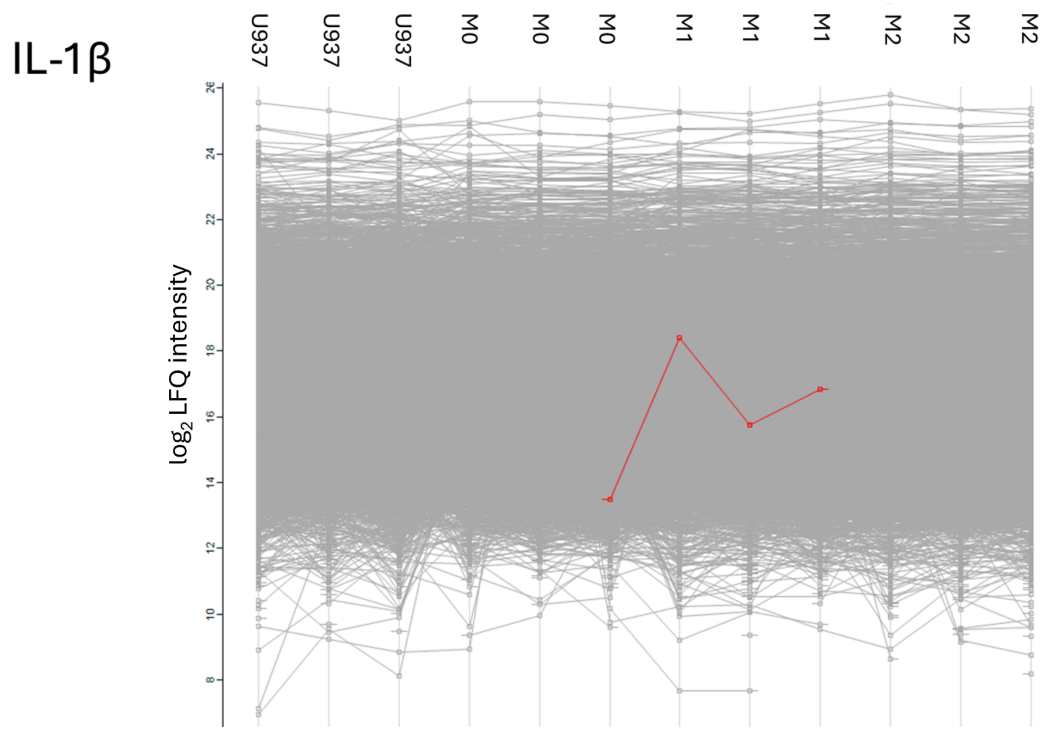

Figure 10: Profile plot of IL-1β $\log_2$ LFQ intensity values of three replicates of each of the U937 differentiation states

Prostaglandin endoperoxide synthase 2 (PTGS2) is an enzyme associated with inflammation and induced by pro-inflammatory signals such as LPS [47]. Macrophages of the pro-inflammatory phenotype induced by LPS treatment showed expression of PTGS2 (figure 11).

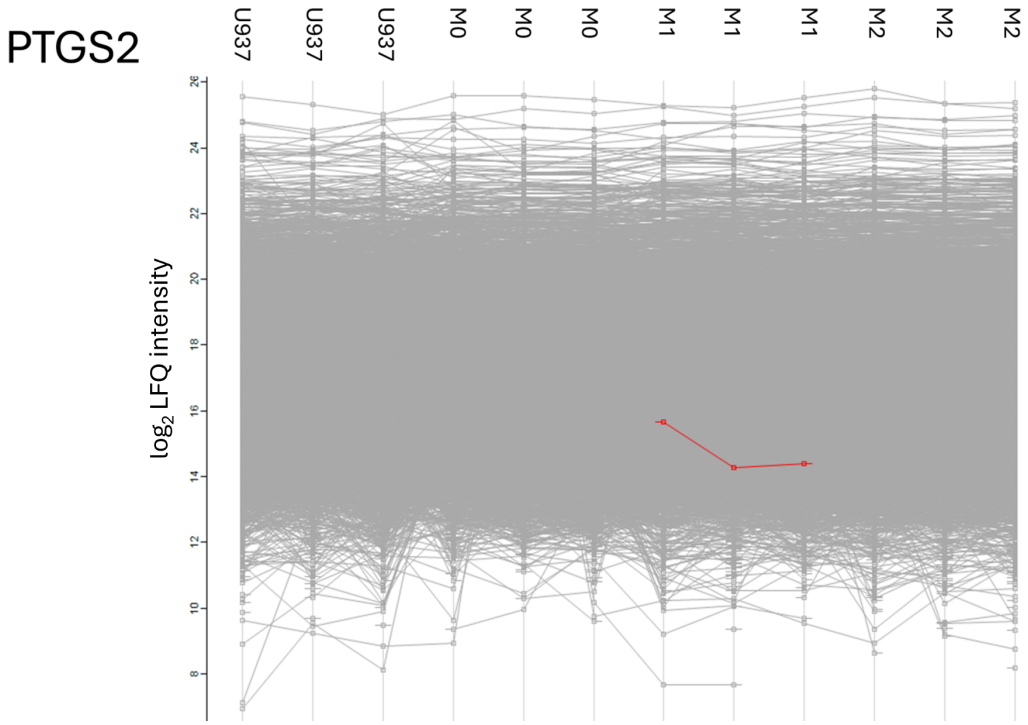

Figure 11: Profile plot of PTGS2 $\log_2$ LFQ intensity values of three replicates of each of the U937 differentiation states

4.3.2 Markers for M2-like Macrophages

As previously described, M2-like macrophages have altered lipid metabolism [34] by expressing proteins such as perilipin-2 (PLIN2) [28] or proteins participating in lipid peroxidation like heme oxygenase 1 (HMOX1). Both of these proteins were expressed in higher amounts in the M2-like macrophage group according to the described polarization protocol (figures 12 and 13).

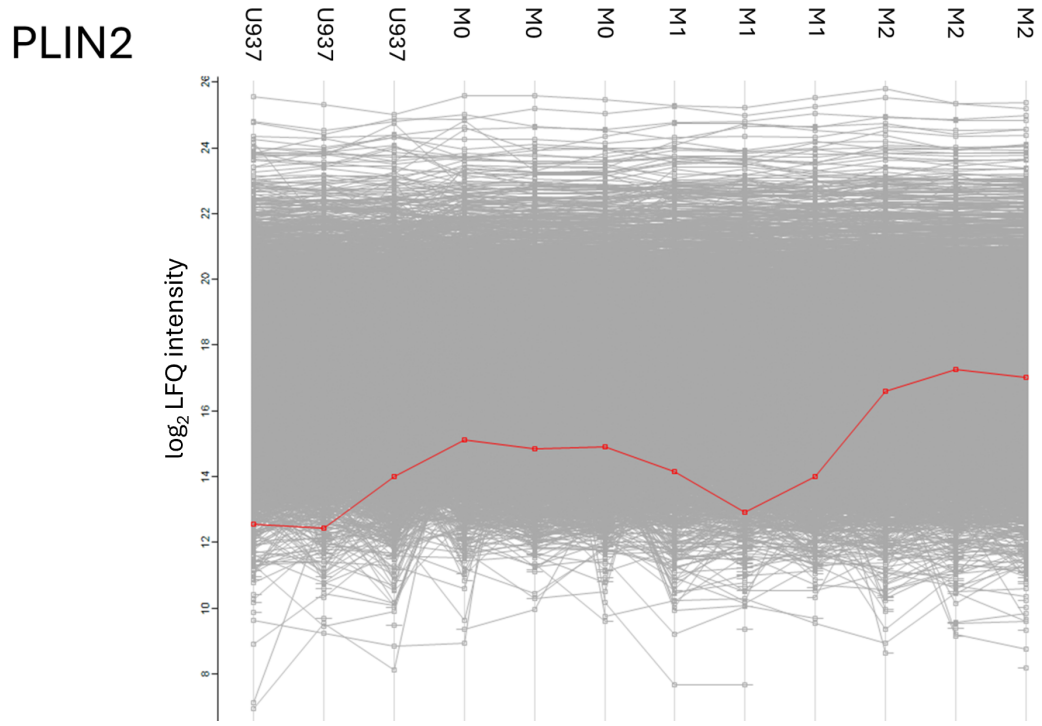

Figure 12: Profile plot of PLIN2 $\log_2$ LFQ intensity values of three replicates of each of the U937 differentiation states

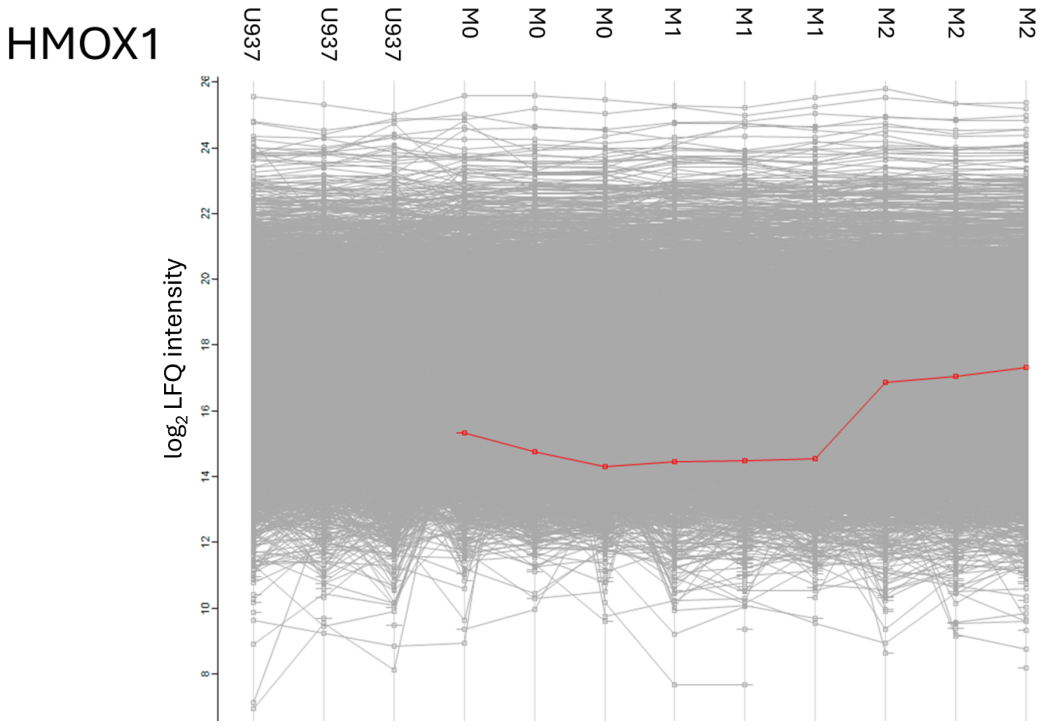

Figure 13: Profile plot of HMOX1 $\log_2$ LFQ intensity values of three replicates of each of the U937 differentiation states

Macrophages of the M2 phenotype can also be identified by the expression of the surface protein CD209 [48][49][50][51]. The differentiation protocol delivered M2-like cells in which significantly higher levels of this surface marker were detected (figure 14).

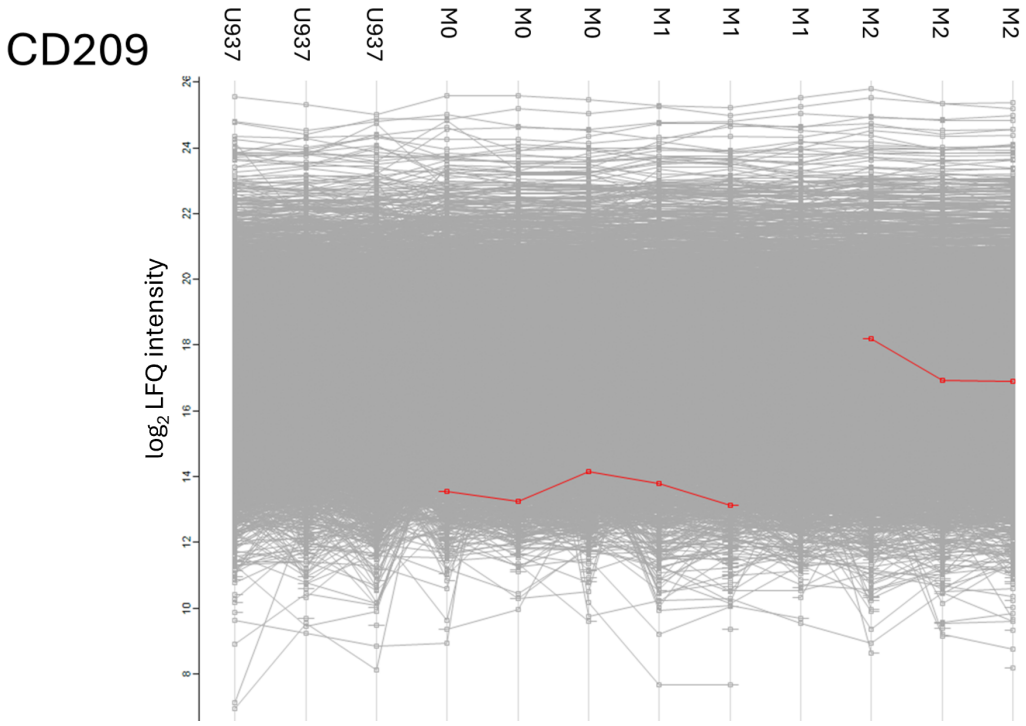

Figure 14: Profile plot of CD209 $\log_2$ LFQ intensity values of three replicates of each of the U937 differentiation states

While the proteomics data was used to ensure that the conducted differentiation protocol delivered macrophages in the desired polarization states, the expression of certain proteins will be shown in the following chapter in combination with the metabolomics data.

4.4 Metabolomics

4.4.1 Data Evaluation

To be able to compare the results of the metabolites from the different samples, the responses had first to be normalized. For this the internal standard succinic acid-d4 was used by calculating the average of all responses in the samples, then for each sample calculating the ratio of the respective succinic acid-d4 level to the average. This was done for SN and WCL separately. The levels of all other metabolites were then normalized to this internal standard by dividing the response value by the ratio of succinic-acid d4 to the average for each respective sample. By normalizing the responses batch effects are eliminated when comparing results from different samples.

There is a time window between sample measurements, which resulted in a batch effect, as can be seen from the responses of the internal standard succinic acid-d4. The second half of samples measured show overall higher succinic acid-d4 responses than the first half (figure 15a), which should also be the case for other metabolites. This effect was due to instrumentation, since normalizing the succinic acid-d4 responses to those of α-ketoglutaric acid-C13, which was added directly before the measurements, eliminates the batch effect (figure 15b). Yet this shouldn't be of problem, since all samples were normalized using their respective succinic acid-d4 response and nearly all metabolites show the same batch effect. Yet certain analytes, namely phenol red, show the opposing trend. Therefore, after normalizing the phenol red responses using succinic acid-d4 the discrepency between the two batches increased. This trend was however the same for SN and WCL, so the subtraction of the SN contamination from the WCL response within a sample was not affected by this phenomenon,

as will be explained next.

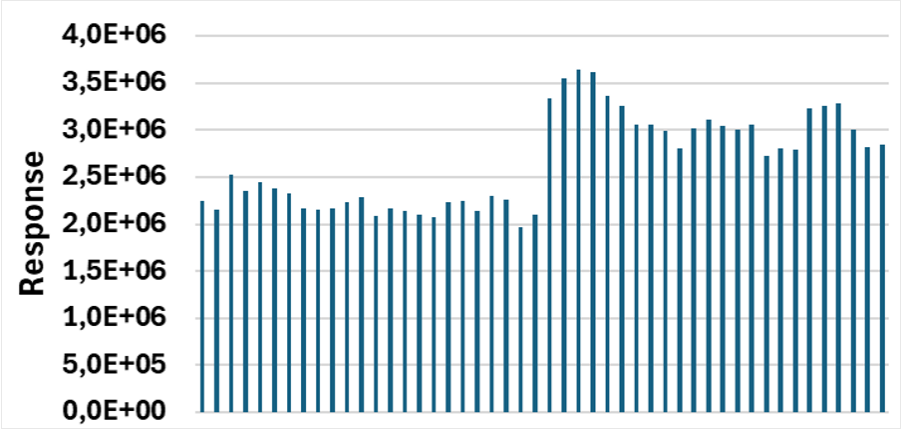

(a) Responses of succinic acid-d4 in all SN samples

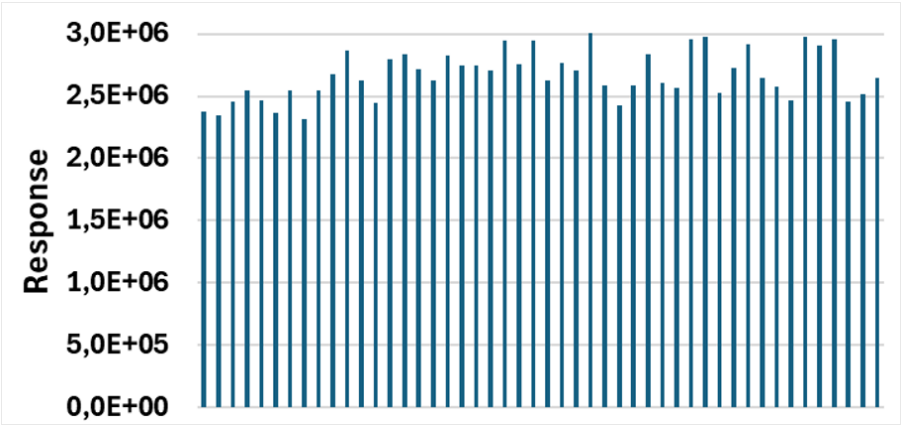

(b) Responses of succinic acid-d4 in all SN samples after normalization to α-ketoglutaric acid-C13

Figure 15: Responses of succinic acid-d4 in all SN samples before and after normalization to α-ketoglutaric acid-C13

As washing cells upon metabolite extraction leads to almost complete loss of certain metabolites (previous unpublished experiments by Slany *et al.*), in the present experiments cells were not washed before lysis. This on the other hand leads to residual SN sticking to the cells, interfering with the responses of metabolites in the WCL. Using the response of phenol red, which is a component of the medium and not present in cells, in WCL samples, the amount of SN contamination can however be determined. In the WCL of the adherent cells the SN contamination is higher than in the floating control U937 cells due to the larger area of contact between the cells and medium in a well of a 6-well plate compared to a cell pellet in a 15 ml centrifugation tube (Falcon), see figure 16.

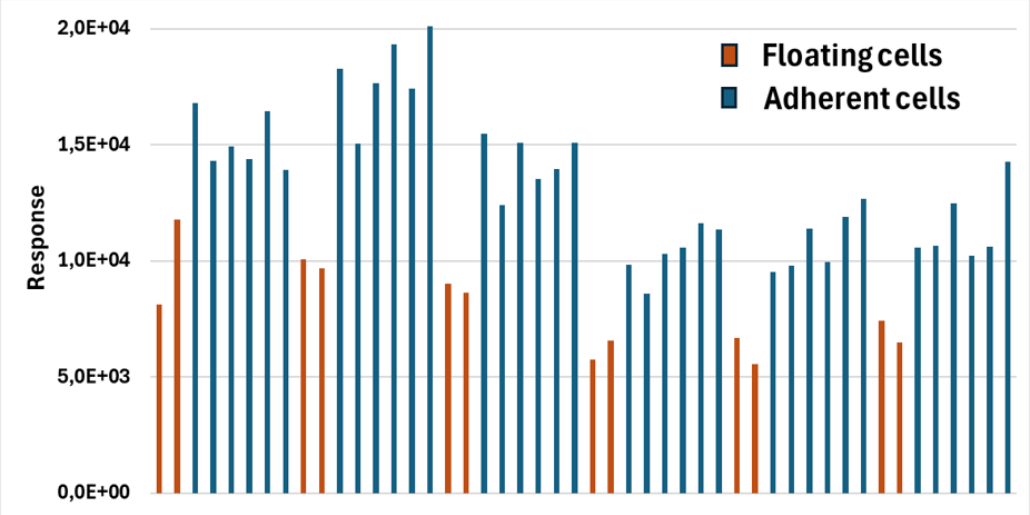

Figure 16: Responses of phenol red in WCL samples due to SN contamination

To correct the metabolite levels obtained in the cells, we decided to subtract the fraction of the respective SN response, obtained from the measurements of phenol red, from the WCL response. Yet for some metabolites the corrected response is negative, since the SN response is far greater than the response in the cell lysate. This could be because SN and WCL present different matrices and therefore have differing matrix effects, leading to suppression or enhancement of certain ions. For example the internal standard α-ketoglutaric acid-C13 showed ion enhancement in WCL compared to the SN, medium and resuspension buffer blanks (figure 17).

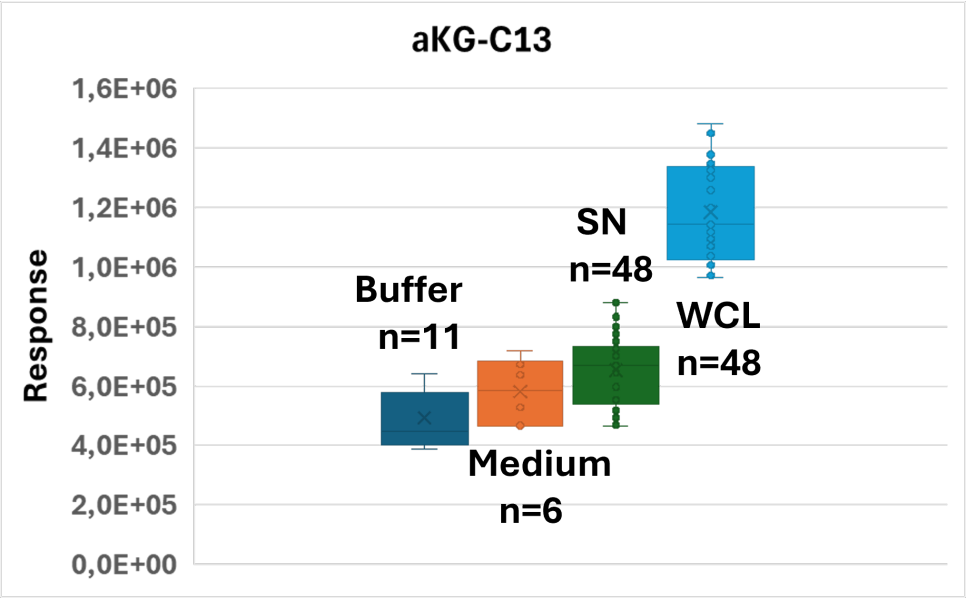

Figure 17: WCL samples showing significantly increased response of α-ketoglutaric acid-C13 compared to SN, medium and resuspension buffer due to ion enhancement in the WCL matrix

A reason could also be that cells may rapidly consume certain metabolites during sample preparation which would explain apparently negative values in WCL. Another reason could be that the response curves of the same analyte in different surroundings changes, for instance, the ion concentration could be in the non-linear area of detection in only one of the matrices, which would lead to the discrepency

in responses. To account for the different matrix effects, calibration curves of certain metabolites could be measured in the different surroundings. This would allow for the determination of the linear and non-linear areas of detection for these analytes in the WCL and SN matrix. Yet doing this for all target metabolites in each matrix may prove to be troublesome. The high amount of SN contamination on the adherent cells also means loss of sensitivity for the detection of analytes in these samples.

Since the cells were cultured for different time periods and therefore had different amounts of time to grow as well as divide to a certain degree, the protein amount in the cells differ between the polarization states. Also due to different cellular functions, different proteins are expressed by the polarized macrophages. Yet these time and functional differences will also have an effect on the amount of metabolites produced by these cell types. To eliminate the effect of differing cell count and size between the different cell types, the metabolite responses in the WCL samples were further normalized to the respective protein amount of the sample. For this, the total protein amount of each WCL sample was determined using Bradford assays, then adjusted to the SN contamination and the average protein amount per well for each cell type was calculated. For each sample the percentage of the protein amount relative to the average was calculated and used for normalization of metabolite responses.

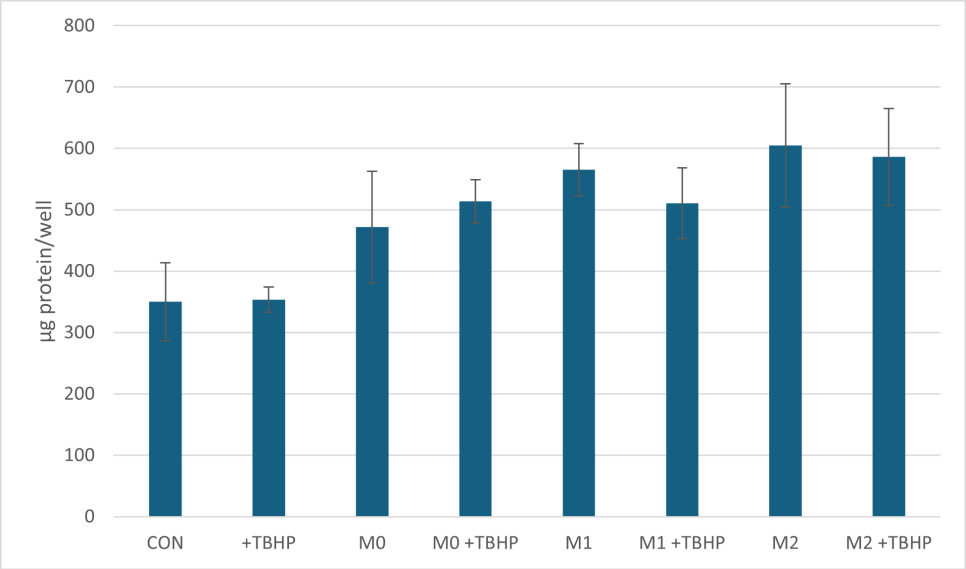

Figure 18: Average WCL protein amount per well of each cell type: U937, M0-, M1- and M2 macrophage

Using the protocol according to figure 2 to differentiate U937 cells leads to different incubation times in the same medium before harvesting the macrophages in different functional states. For instance, M0 macrophages were in the same medium for 3 days before being harvested, while M1-like macrophages were in medium for 2 days, whereas the M2-like and control cells for only 1 day. This means that differences in the amount of a metabolite that was secreted from the cells into the medium, or the amount of a molecule that was used up from the medium, could stem from one cell type being longer in culture than the others and not necessarily from actual functional differences.

When analyzing a complex micture of analytes from cells using LC-MS, certain metabolites may elute at the same time and have similar transitions in the QQQ. This impedes on metabolomics analysis trying to discern between changes in metabolism. Additionally, a general issue is the lack of stability of metabolites, which allows them to degrade in the autosampler during the time it takes for an LC-MS measurement and even when stored at -80 °C.

4.4.2 PCA Plots

The corrected responses of all analytes were used to create PCA plots of all SN and WCL samples.

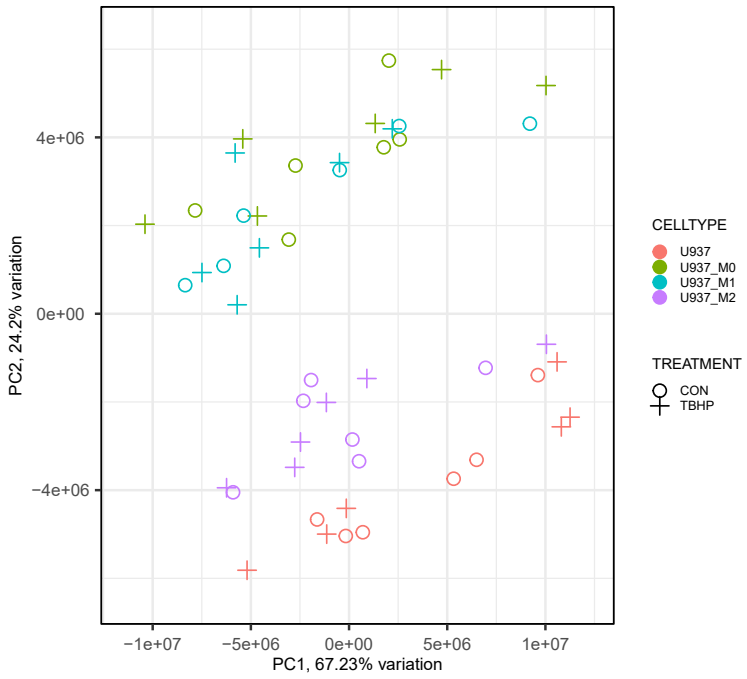

(a) PCA plot of SN samples

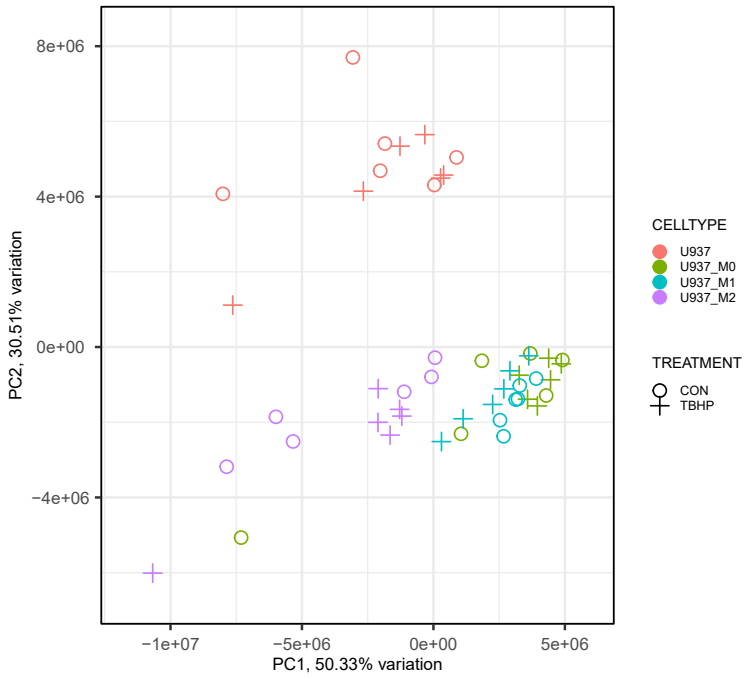

(b) PCA plot of WCL samples

Figure 19: PCA plots of all SN and WCL samples using corrected metabolite responses. Depicted are the replicates of each cell type: U937, M0-, M1- and M2 macrophage each with or without 100 µM TBHP treatment

Looking at figures 19a and 19b it can be seen that for the SN and WCL the control U937 cells and M2 macrophages form separate clusters, whereas the M0- and M1-like phenotypes seem to not differ much metabolically. This could hint towards PMA already acting somewhat as an inflammatory stimulus leading to the naive macrophages already expressing pro-inflammatory properties. This coincides with the proteomics results, in which fewer proteins are significantly regulated in the M1 macrophages relative to the M0 macrophages compared to the number of significantly regulated proteins between the other cell types and the M0 macrophages. Additionally, the treated and untreated groups don't seem to cluster differently from one another, showing that applying oxidative stress using TBHP did not induce significant changes in the metabolome of these cell types.

4.4.3 Kynurenine Pathway

Herein, the metabolic pathway of kynurenine in macrophages, which includes tryptophan and its metabolites, was analyzed, since many tryptophan catabolites have immunomodulatory activity in immune cells [52]. Tryptophan can be broken down by indoleamine 2,3-dioxygenase 1 (IDO1) into kynurenine or by interleukin-4-induced-1 (IL4I1) to indole-3-pyruvic acid (I3P) both of which can further be transformed into kynurenic acid [53], see figure 20.

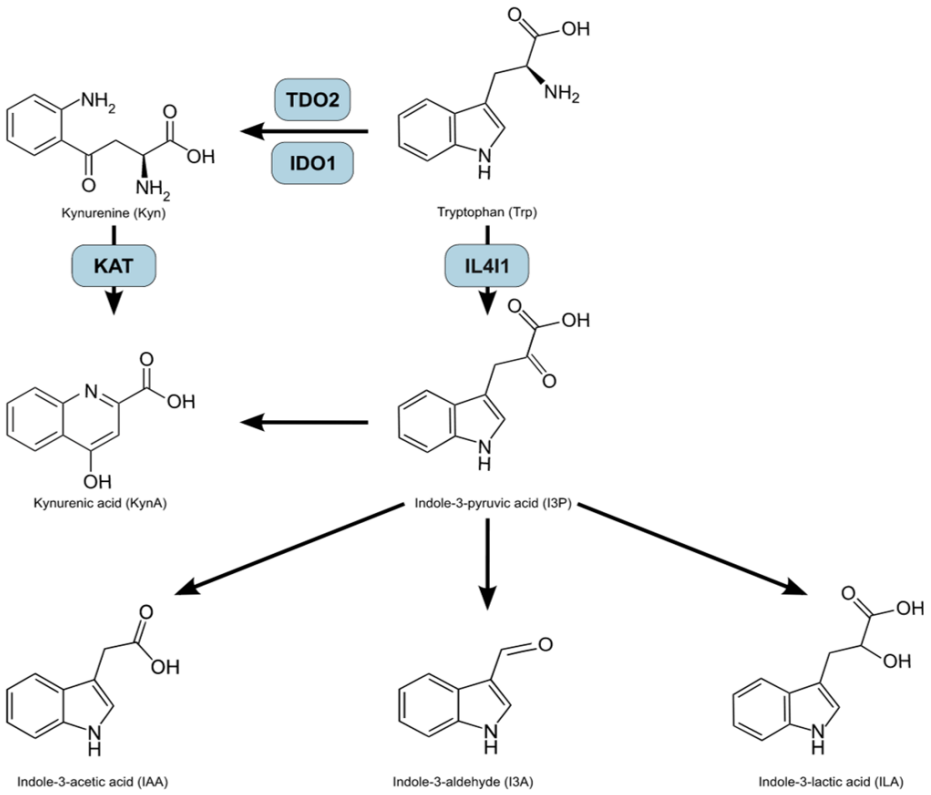

Figure 20: Tryptophan catabolism to kynurenine by IDO1 and I3P by IL4I1, which are further metabolized to kynurenic acid. I3P has other downstream metabolites such as ILA. This figure was adapted with permission from [53]

This catabolic process releases kynurenine from the cells which acts anti-inflammatory [33] and presents an extracellular antioxidant defense during inflammation [54]. The enzyme IL4I1 has also been described to regulate macrophage polarization by shifting it towards the M2-like phenotype [55] in addition to its product I3P acting anti-inflammatory [56].

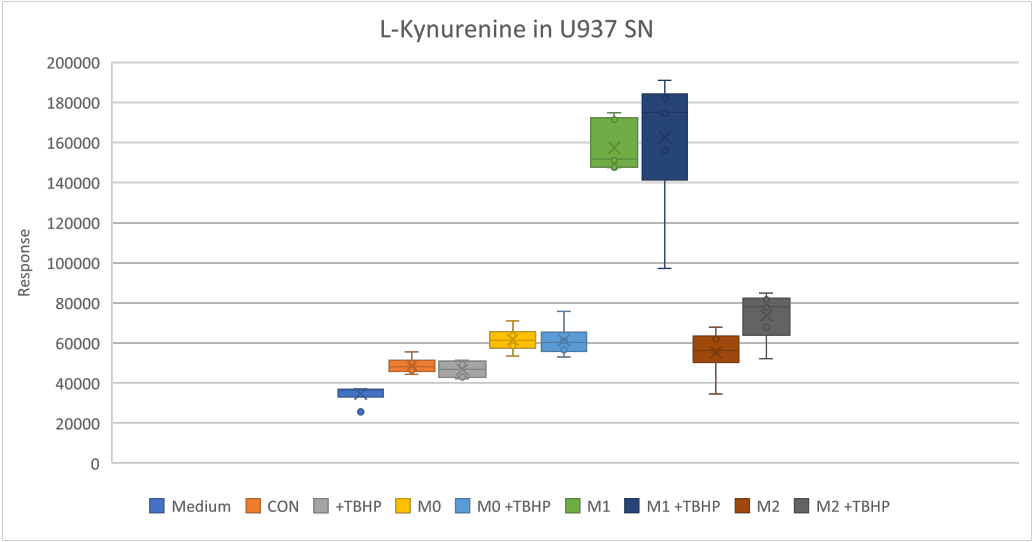

Figure 21: Relative levels of kynurenine in six SN replicates of U937 cells, M0-, M1- and M2 macrophages treated with and without 100 µM TBHP as well as base level in medium

Yet looking at the determined relative amounts in differently polarized macrophages, it can be seen that the inflammatory activated cells secrete more kynurenine than the M2 macrophages (figure 21), which opposes the suspected anti-inflammatory character of this metabolite.

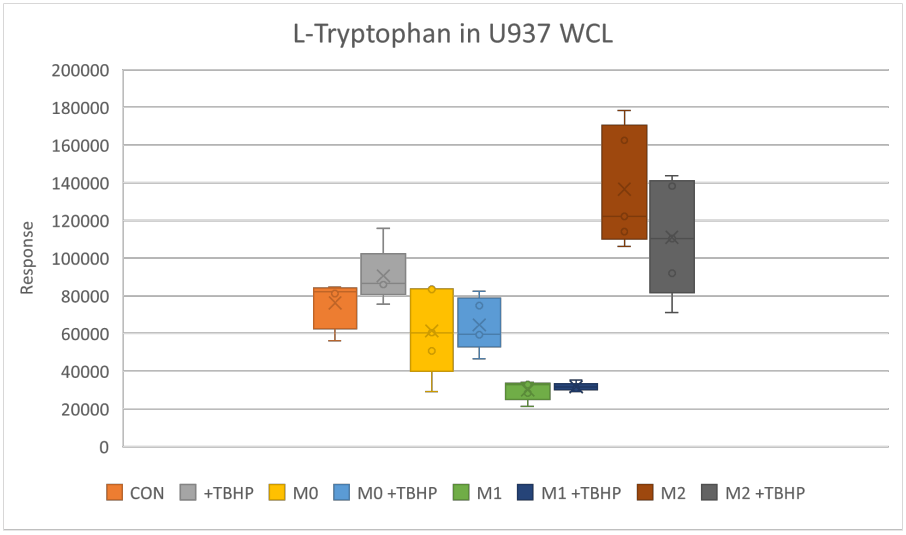

(a) Relative levels of tryptophan in six WCL replicates of U937 cells, M0-, M1- and M2 macrophages treated with and without 100 µM TBHP

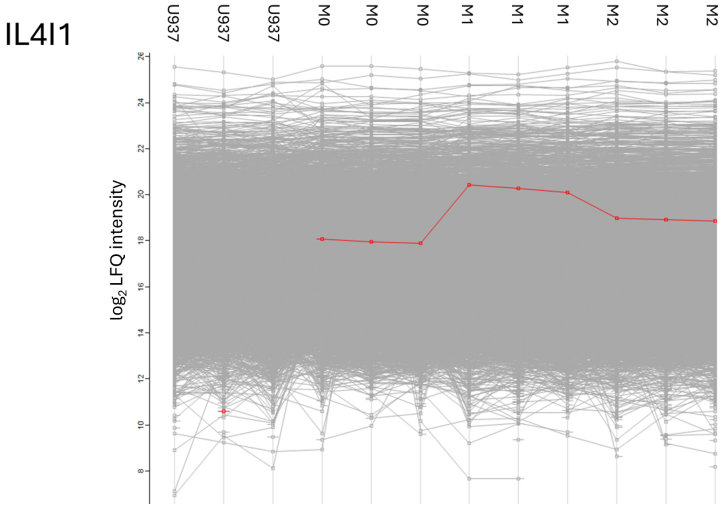

(b) Profile plot of IL4I1 $\log_2$ LFQ intensity values of three replicates of each of the U937 differentiation states

Figure 22: Relative levels of tryptophan in WCL of U937 cells, M0-, M1- and M2 macrophages treated with and without TBHP as well as IL4I1 in WCL of all cell types

Looking at figure 22b it can be seen that M1 macrophages express higher amounts of IL4I1 than M0- and M2 macrophages. This would lead to higher catabolism of tryptophan in the M1 polarized macrophages, which is the case looking at the diminished tryptophan level in M1 macrophages in figure 22a. This seemingly opposing trend of higher breakdown of tryptophan to anti-inflammatory metabolites in macrophages of the pro-inflammatory type has also been reported by Xue et al. [57]. This also coincides with the higher amount of the product of IL4I1 I3P in the M1 macrophages compared to the M2 macrophages (figure 23).

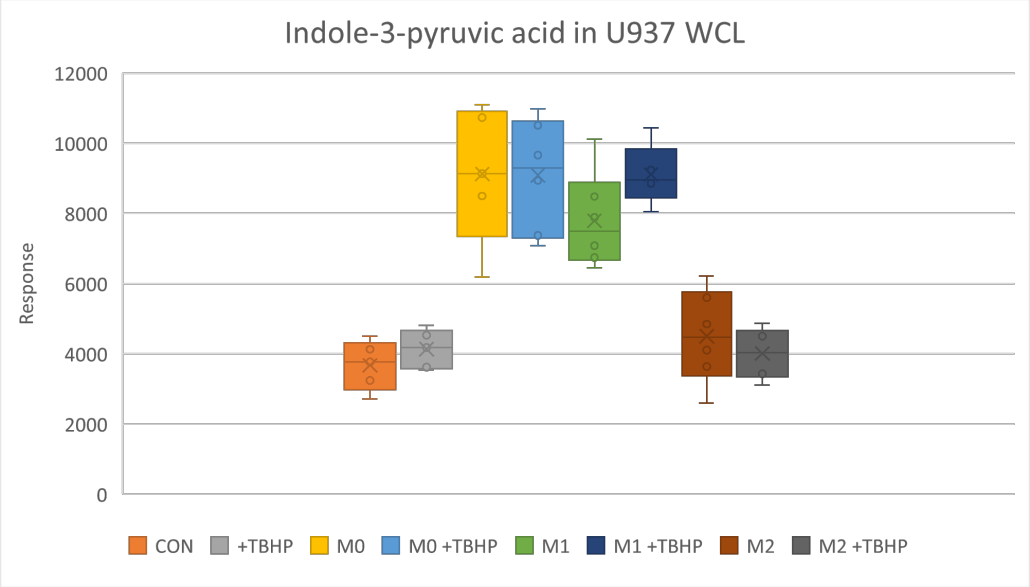

Figure 23: Relative levels of indole-3-pyruvic acid in six WCL replicates of U937 cells, M0-, M1- and M2 macrophages treated with and without 100 µM TBHP

Interestingly, the downstream product of I3P indole-3-lactic acid (ILA) [53] (figure 20) seems to occur in higher concentrations in the M2-like cells rather than the M1 macrophages with higher tryptophan catabolism (figure 24). It is important to keep in mind, that due to the high turnover of metabolites, metabolomics merely acts as a snapshot of reality representing only one time point of a metabolic pathway, for instance, the product being increased while the precursor is decreased. So the level of the downstream product ILA can be higher in the M2 macrophages (figure 24) while the level of the upstream metabolite I3P is lower (figure 23) and vice versa in M1-like macrophages since in the former cells the I3P reacted further to ILA.

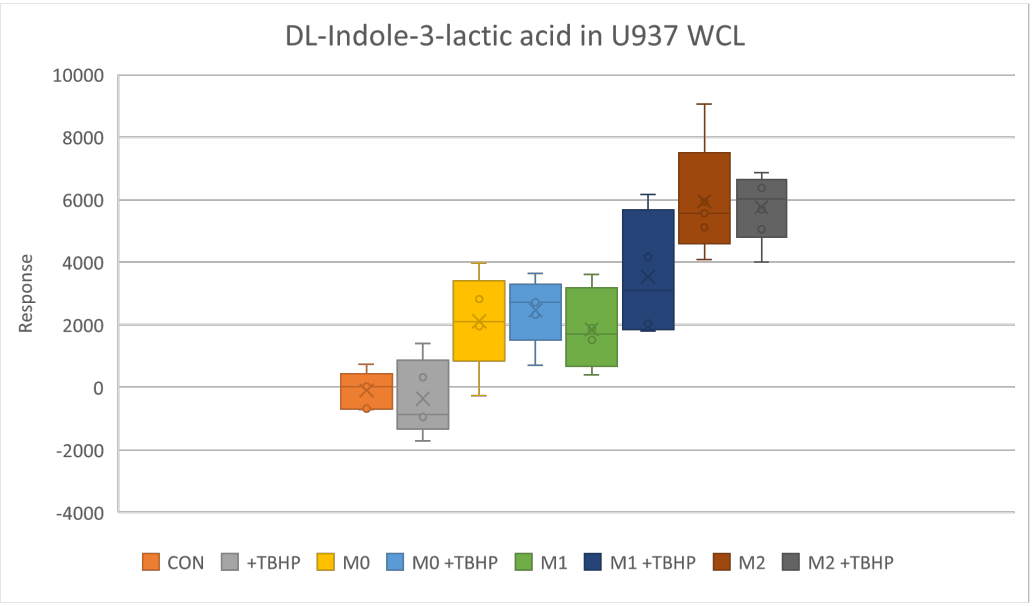

Figure 24: Relative levels of indole-3-lactic acid in six WCL replicates of U937 cells, M0-, M1- and M2 macrophages treated with and without 100 µM TBHP

Kynurenine can further be metabolized by kynurenine 3-monoxygenase (KMO) to 3-hydroxykynurenine

which in turn is transformed into 3-hydroxyanthranilic (3-HAA) acid by kynureninase (KYNU) [58]. It has been reported that 3-HAA is synthesized and released by macrophages leading to anti-inflammatory effects [52][54] as well as being an immunosuppressant [59]. Yet looking at the obtained results, it can be seen that the pro-inflammatory M1 macrophages overexpress KYNU and secret higher levels of 3-HAA rather than the anti-inflammatory M2 macrophages (figure 25).

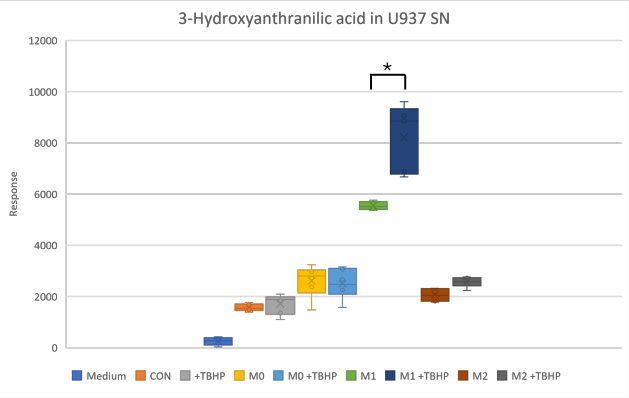

(a) Relative levels of 3-HAA acid in SN of U937 cells, M0-, M1- and M2 macrophages treated with and without 100 µM TBHP as well as base level in medium. * $p < 0.01$

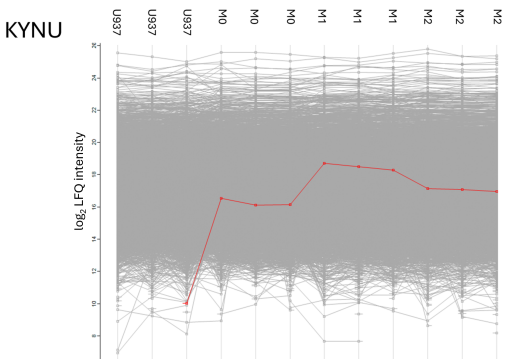

(b) Profile plot of KYNU $\log_2$ LFQ intensity values of three replicates of each of the U937 differentiation states

Figure 25: Relative levels of 3-HAA acid in SN of U937 cells, M0-, M1- and M2 macrophages treated with and without TBHP as well as KYNU in WCL of all cell types

As previously mentioned the polarization of macrophages is to be seen as a gradient with the states being interchangable. This is highlighted by the mentioned results showing one metabolic pathway isn't merely reserved for one functional state. The cells in culture can also differ from the intended differentiation path and can functionally be found somewhere in between the two extremes, therefore presenting a hybrid of pro- and anti-inflammatory characteristics. This makes it hard to discern between pro- and anti-inflammatory pathways and not being able to assign these reactions to specific cellular states. Additionally, metabolic pathways are intertwined and the concentration of one metabolite being diminished or increased could lead to or be caused by a different metabolic pathway. And markers being increased in inflammatory or anti-inflammatory macrophages don't necessarily mean that these cause inflammatory or anti-inflammatory effects but could rather be a consequence of cells trying to keep homeostasis. The complex interplay of metabolites and effects on cellular level make it difficult to discern whether metabolism if the effect or effector of the observed cell functionality. For instance, interferon-gamma, a pro-inflammatory cytokine [60], induces IDO1 which leads to the production of kynurenine [61][53], therefore pro-inflammatory macrophages can eventually respond to the inflammatory stimulus and produce anti-inflammatory modulators in cell culture experiments. Figuratively, their functional state moves more towards the M2-like phenotype along the polarization gradient.

4.4.4 Glycolysis

As previously stated, M1 macrophages rely on increased glycolysis for their energy household [33][62]. Dihydroxyacetone phosphate (DHAP) is an intermediate in the glycolytic breakdown of glucose [63]. Looking at figure 26, it can be seen that DHAP is detected in higher amounts in M1-like cells than in

control, M0- and M2-like cells.

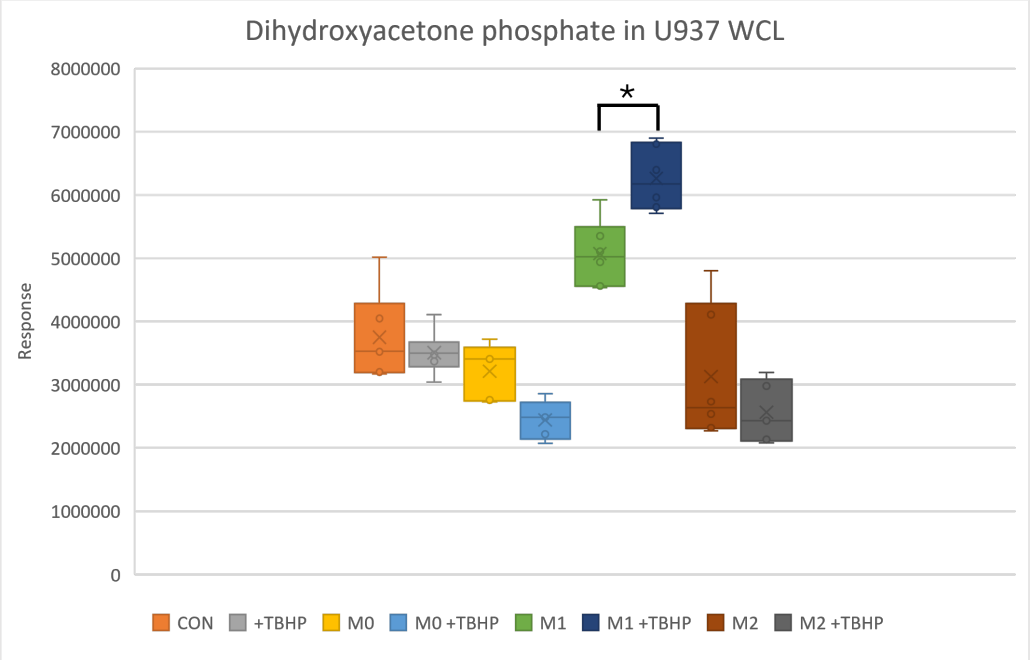

Figure 26: Relative levels of DHAP in six WCL replicates of U937 cells, M0-, M1- and M2 macrophages treated with and without 100 µM TBHP.
* $p < 0.01$

Fructose-1,6-biphosphate is also an intermediate in glycolysis and also occurs in higher concentrations in M1-like macrophages (figure 27), hinting towards increased glycolytic activity in the intended M1-like cells.

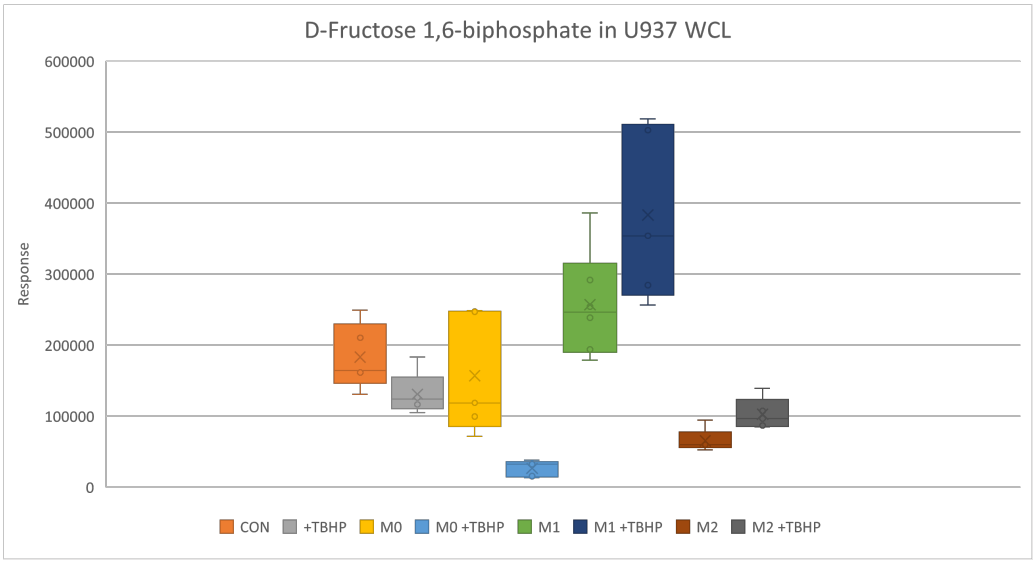

Figure 27: Relative levels of fructose-1,6-biphosphate in six WCL replicates of U937 cells, M0-, M1- and M2 macrophages treated with and without 100 µM TBHP

4.4.5 Glutaminolysis

M2 macrophages rely on oxidative phosphorylation and fatty acid oxidation to fuel their ATP synthesis [33][34]. These cells use glutaminolysis to generate ∝-ketoglutarate which is essential for these two

metabolic pathways as well as directly promoting M2 polarization [33]. The first enzyme in this reaction is glutaminase (GLS), which converts glutamine to glutamate [64]. The proteomics data show this protein being expressed at higher rates in cells of the M2 phenotype (figure 28).

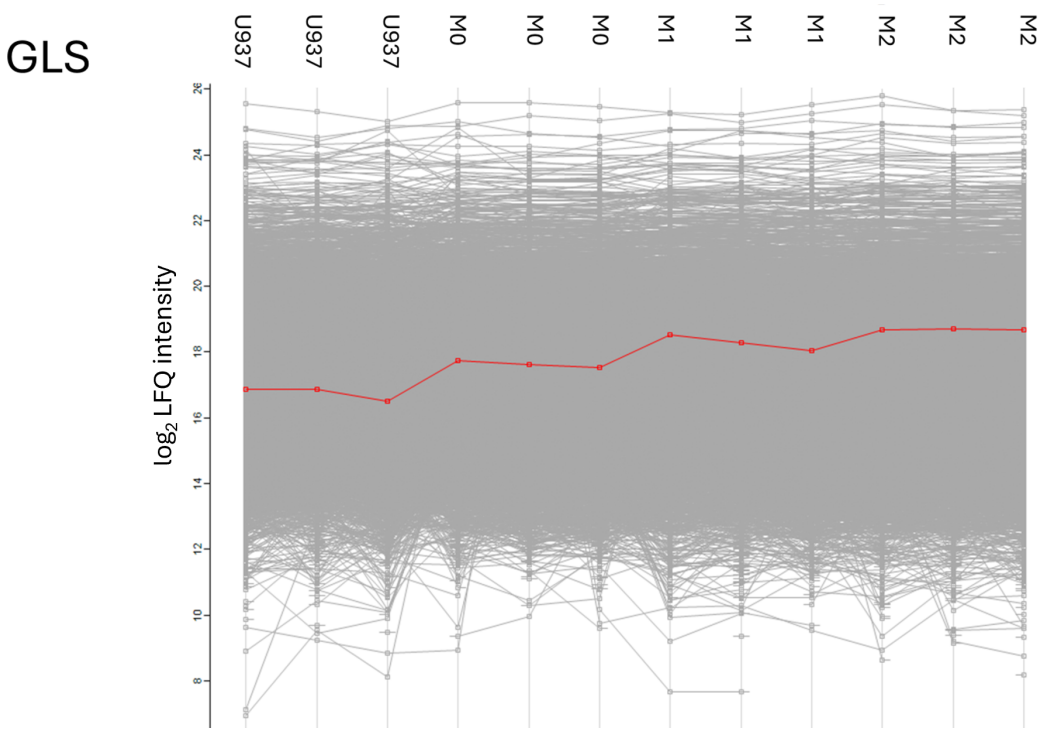

Figure 28: Profile plot of GLS $\log_2$ LFQ intensity values of three replicates of each of the U937 differentiation states

When looking at the levels of glutamine in the different cell types, M2-like cells show negative glutamine levels in the WCL (figure 29a). Taking into account the previously mentioned considerations when subtracting the SN contamination from the WCL response, the reason for the negative value could be very low concentrations of glutamine in the M2 macrophages due to increased glutaminolysis. Additionally, at the point when harvesting the cells they do not have any access to nutrients which could mean an even higher consumption of glutamine and therefore a negative response value after subtracting the SN part. The reason for M0 and M1 macrophages using more glutamine from the medium than M2 macrophages (figure 29b) can be due to the longer time period of those cells spent in the same cell culture medium before extracting the metabolites rather than functional differences.

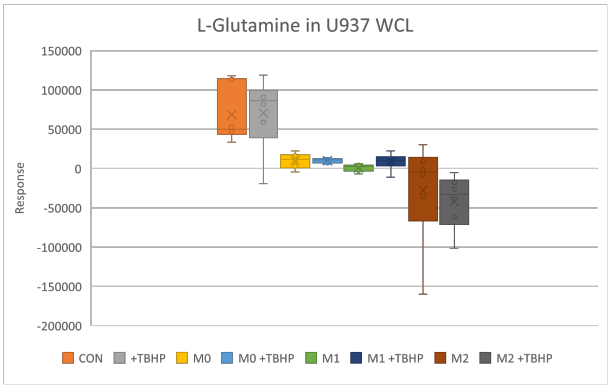

(a) Relative levels of glutamine in six WCL replicates of U937 cells, M0-, M1- and M2 macrophages treated with and without 100 µM TBHP

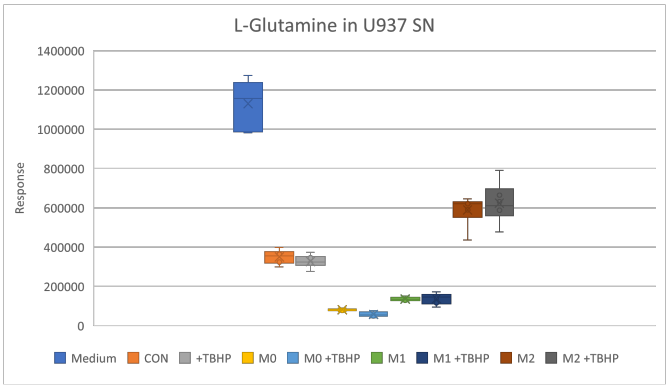

(b) Relative levels of glutamine in six SN replicates of U937 cells, M0-, M1- and M2 macrophages treated with and without 100 µM TBHP as well as base level in medium

Figure 29: Relative levels of glutamine in WCL and SN of U937 cells, M0-, M1- and M2 macrophages treated with and without TBHP

Fitting to the notion that M2 macrophages perform glutaminolysis, while the M0 and M1 macrophages do not [62], the levels of products of glutaminolysis, namely glutamate and α-ketoglutarate are increased in M2-like cells (figures 30 and 31).

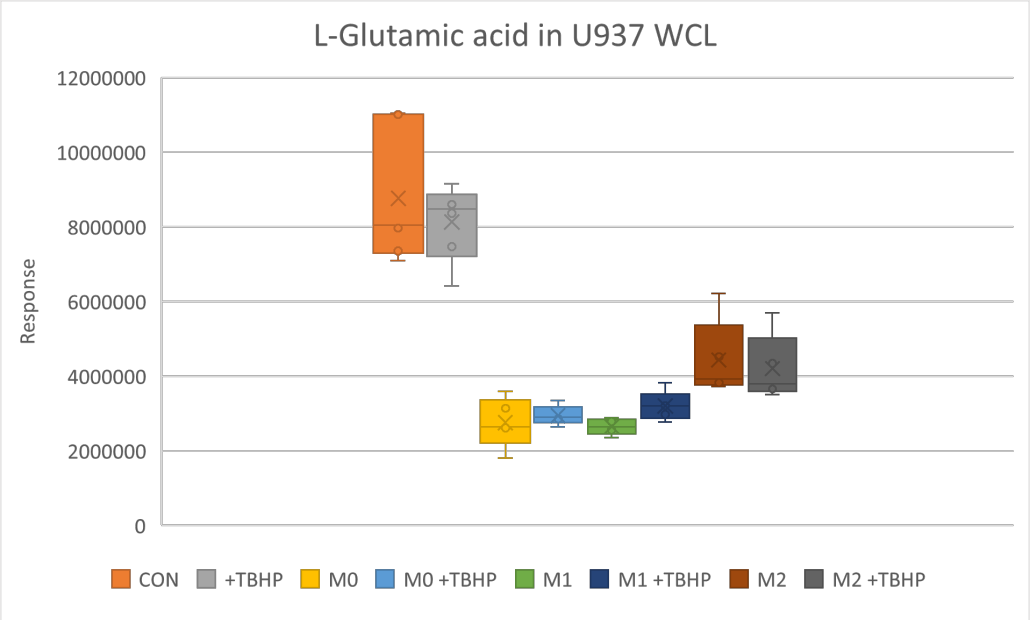

Figure 30: Relative levels of glutamic acid in six WCL replicates of U937 cells, M0-, M1- and M2 macrophages treated with and without 100 µM TBHP

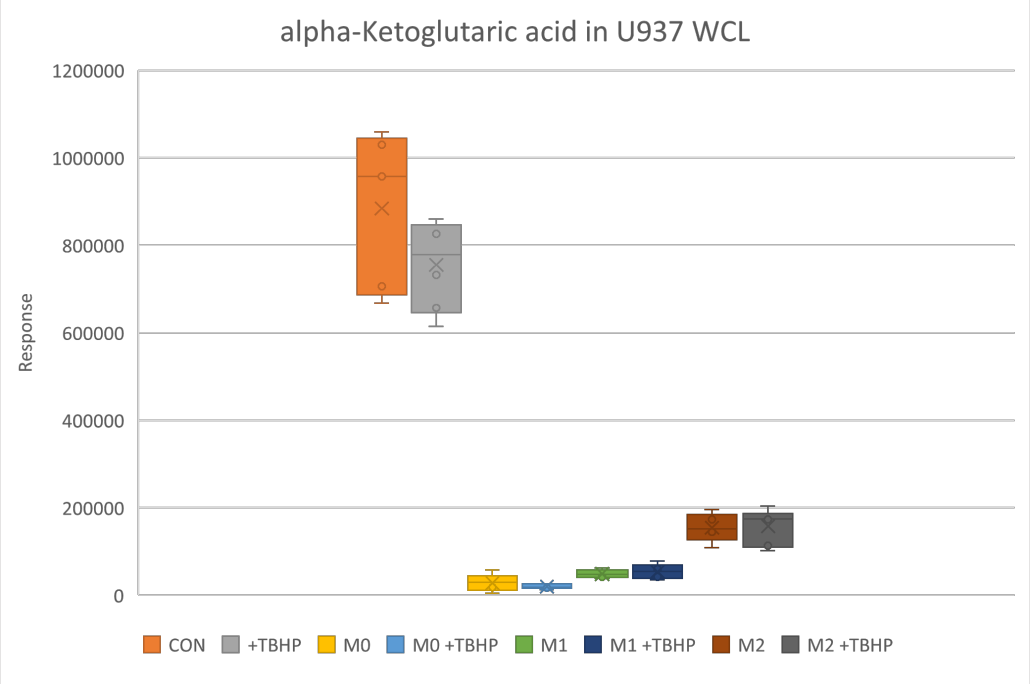

Figure 31: Relative levels of α-ketoglutaric acid in six WCL replicates of U937 cells, M0-, M1- and M2 macrophages treated with and without 100 µM TBHP

Another reason for the decreased level of α-ketoglutarate in M1 macrophages (figure 31) could be the remodeled TCA cycle, which leads to less formation of α-ketoglutarate [65]. This highlights the complex intertwinement of cellular metabolic pathways and their respective products.

4.4.6 Additional Metabolic Markers

Malic acid has been reported to act inhibitory on macrophages polarizing towards the M1 state [66] while also being able to drive polarization towards the M2 macrophage phenotype [67]. Coinciding with this, the level of malic acid is higher in cells of the intended M2-like group while being lower in the M1 polarized macrophages (figure 32).

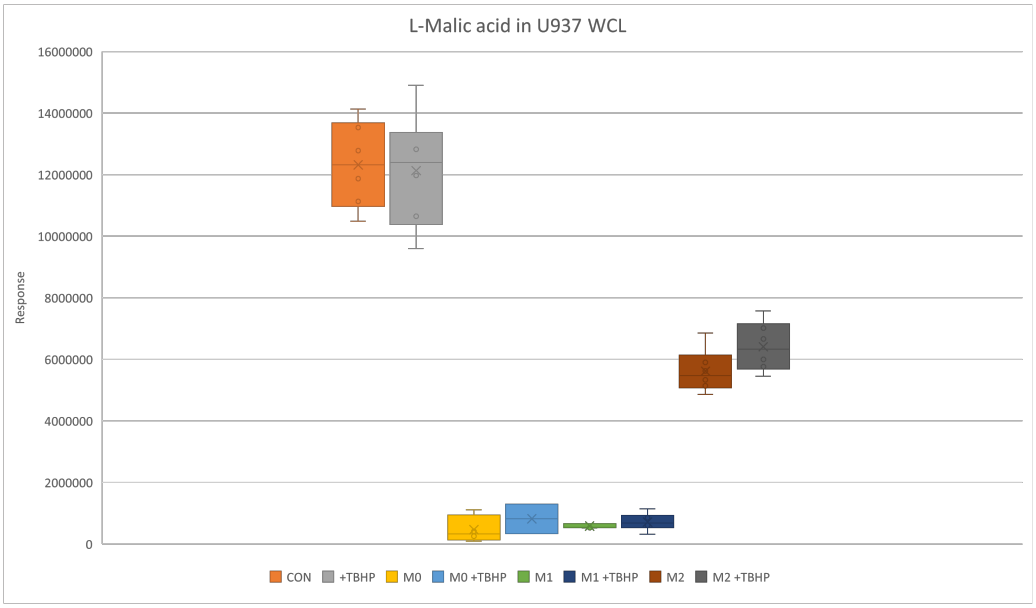

Figure 32: Relative levels of malic acid in six WCL replicates of U937 cells, M0-, M1- and M2 macrophages treated with and without 100 µM TBHP

O-phospho-L-serine, which is the head-group of the abundant phospholipid phosphatidylserine, has shown to induce immune cells to secrete immunosuppressive cytokines [68]. Furthermore, phosphatidylserine has been described to have an anti-inflammatory function [69]. Fittingly, this compounds levels are higher in cells of the immunosuppressive M2-like phenotype compared to the pro-inflammatory M1 macrophages (figure 33).

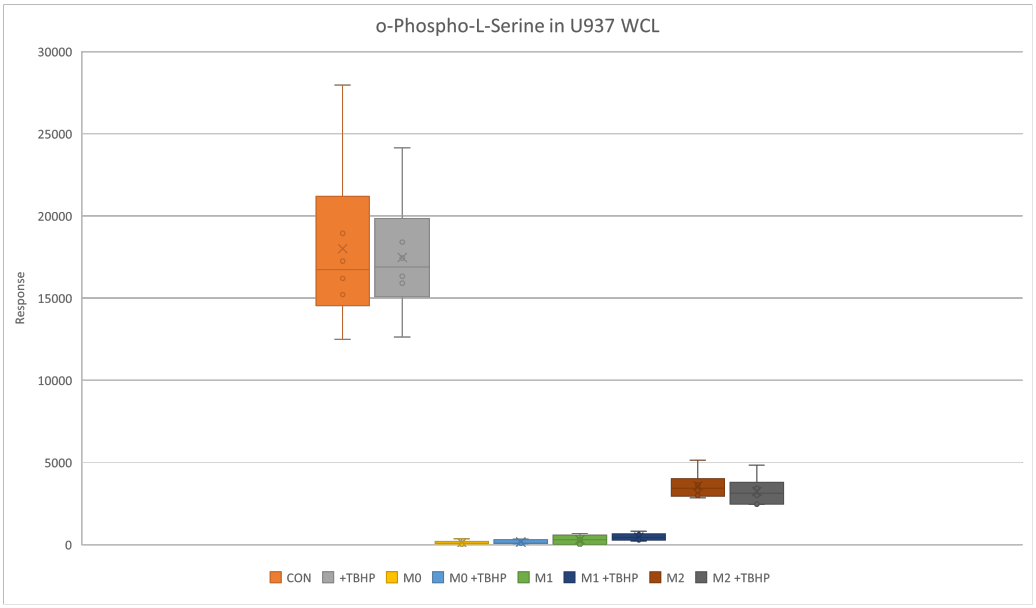

Figure 33: Relative levels of o-phospho-L-serine in six WCL replicates of U937 cells, M0-, M1- and M2 macrophages treated with and without 100 µM TBHP

Pantothenic acid, commonly called vitamin B5, has been reported to increase the phagocytic capability as well as enhance the inflammatory response in macrophages [70]. Befittingly, this metabolites levels are higher in M1 macrophages compared to M2 macrophages (figure 34). As previously shown by the PCA plots, M0 and M1 macrophages are metabolically similar (figures 19a and 19b), which is

highlighted by, for instance, them showing similar signatures of pantothenic acid (figure 34).

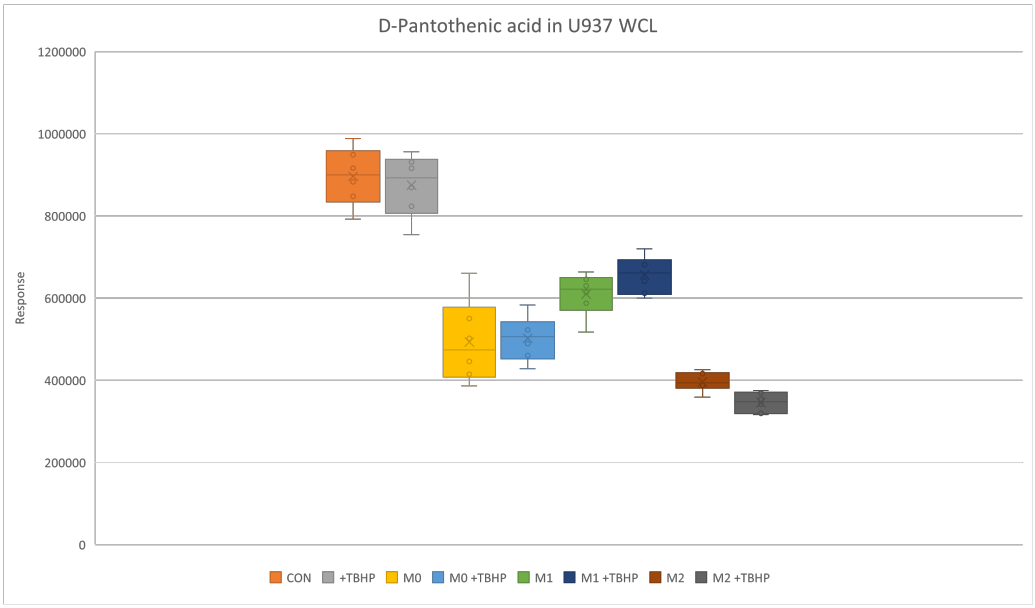

Figure 34: Relative levels of pantothenic acid in six WCL replicates of U937 cells, M0-, M1- and M2 macrophages treated with and without 100 µM TBHP

4.4.7 Effects of ROS Stress on the Metabolism of Macrophages

As previously shown by the MTT and cell counting assays, TBHP presents minimal effects on the cells due to cellular defense mechanisms and the fast reaction time of ROS. This is also exhibited by the minimally differing levels of oxidized glutathione, which is an antioxidant peptide with ROS scavenging capability [71], in the TBHP treated and untreated groups at the time of harvesting the cells (figure 35).

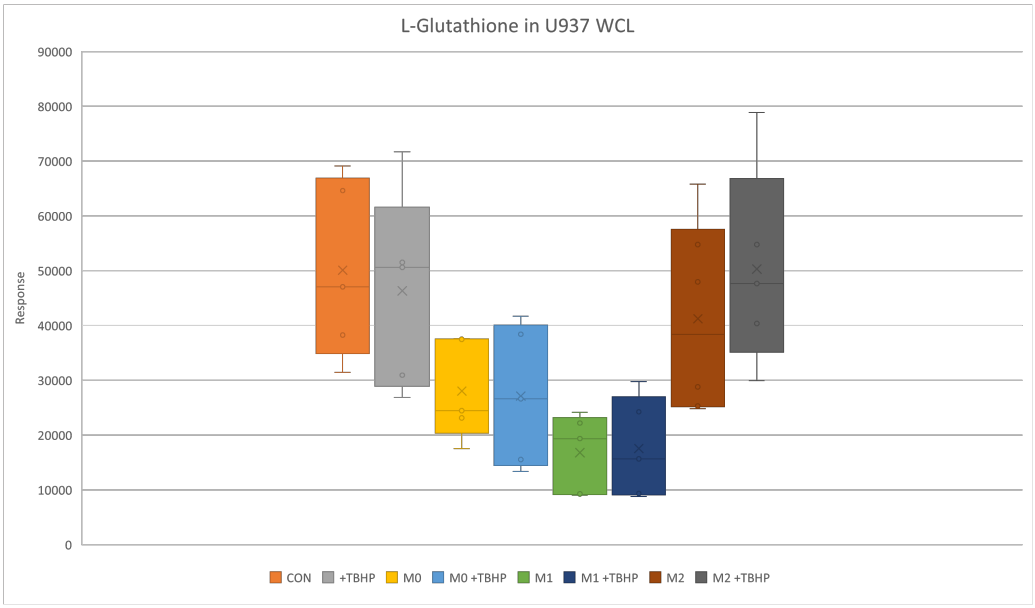

Figure 35: Relative levels of oxidized glutathion in six WCL replicates of U937 cells, M0-, M1- and M2 macrophages treated with and without 100 µM TBHP

Similarly the precursor to glutathione γ-glutamylcystein (γ-Glu-Cys) shows no effects of ROS in the TBHP treated groups (figure 36). The reason for this could be the self-defense mechanisms against oxidative stress intrinsic to macrophages shown by the expression of proteins to protect the cells from ROS (figures 37 and 38). On the other hand this could show how the cells are able to recover from oxidative damage after a long period of time exceeding the fast reaction time of ROS or how the TBHP is buffered out in the medium not leading to any impact on the cells.

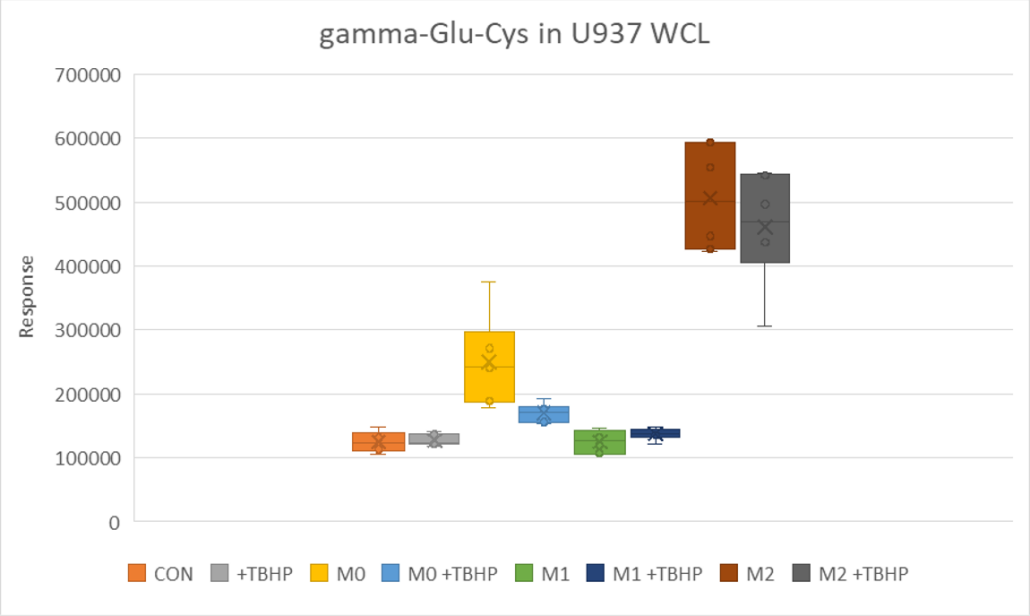

Figure 36: Relative levels of γ-Glu-Cys in six WCL replicates of U937 cells, M0-, M1- and M2 macrophages treated with and without 100 µM TBHP

Additionally, figures 35 and 36 show the higher levels of antioxidants correlated with M2 macrophages [11]. These peptides have anti-inflammatory effects in addition to γ-glutamylcystein being able to inhibit LPS-based inflammatory signaling [72][73]. On the other hand, it has been described that the inflammatory response induced by LPS leads to the breakdown of the γ-glutamylcystein producing enzyme in macrophages [74], which could also be the reason for the decreased levels of this peptide in the M1 macrophages (figure 36). This underlines how an observed metabolic signature can either be the result of a cells functional state or the cause of the presented phenotype and how it is difficult to differentiate between the two. Another antioxidant that is overexpressed in M2 macrophages is glutathione peroxidase 1 (GPX1) [11] (figure 37), which eliminates ROS using glutathion [75].

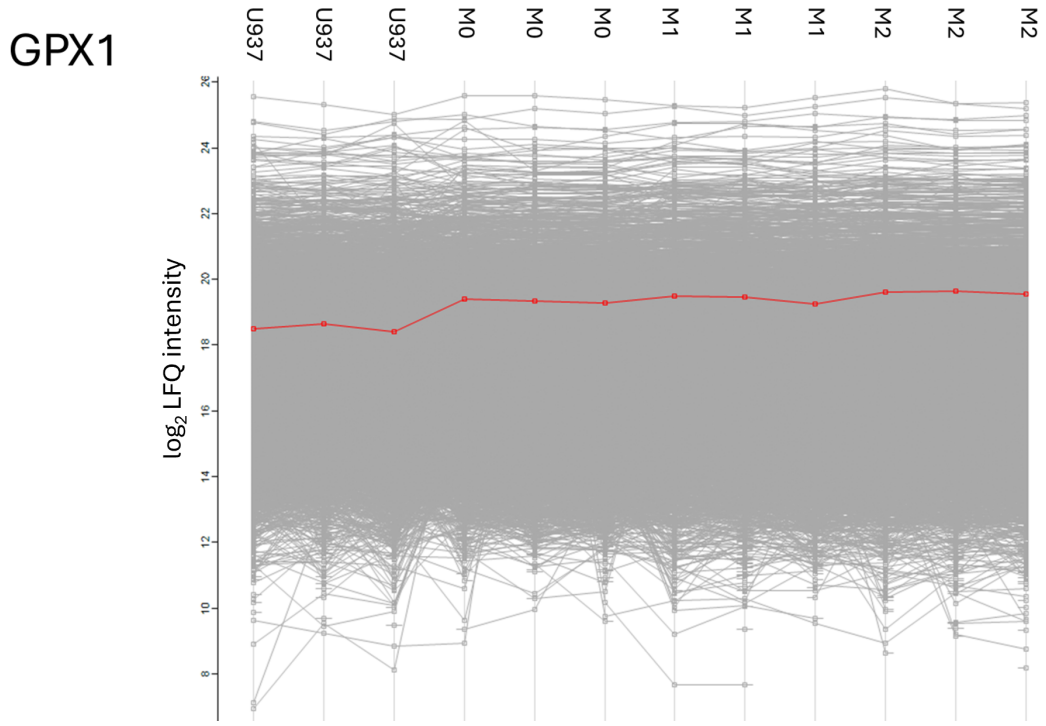

Figure 37: Profile plot of GPX1 $\log_2$ LFQ intensity values of three replicates of each of the U937 differentiation states

On the other hand the production of another ROS defense mechanism, superoxide dismutase 2 (SOD2), which scavenges superoxide radicals in a non-glutathione dependent manner [76], is significantly increased in M1-like macrophages (figure 38).

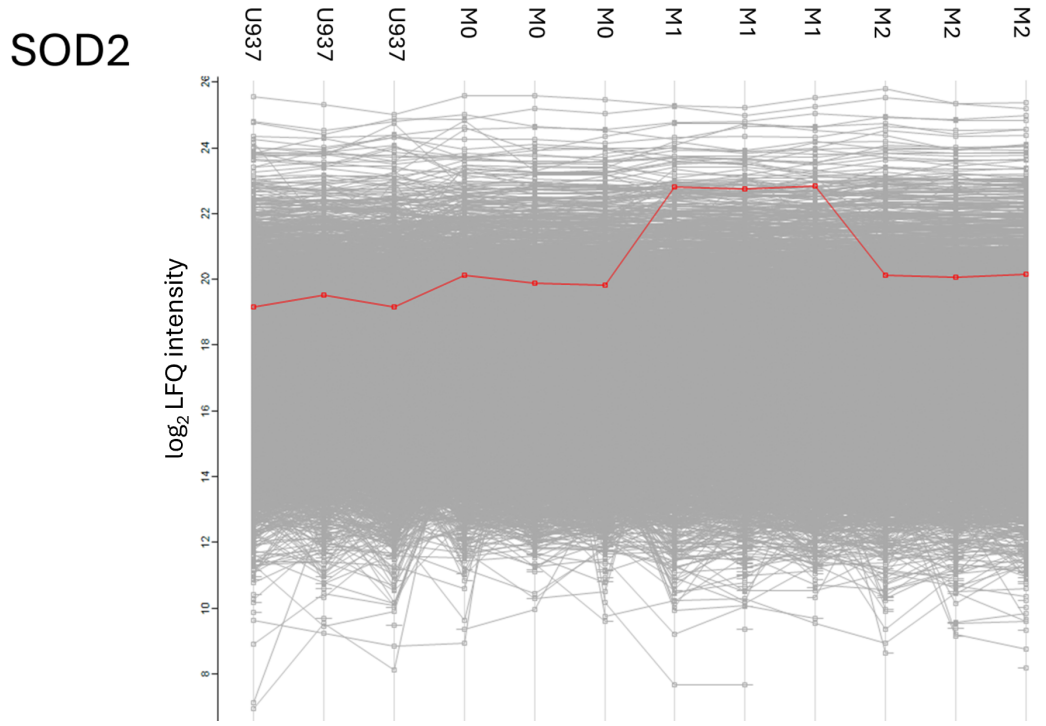

Figure 38: Profile plot of SOD2 $\log_2$ LFQ intensity values of three replicates of each of the U937 differentiation states

Interestingly these protective proteins are also expressed in the undifferentiated U937 cells, which in

the MTT assays showed higher vulnerability towards TBHP at an IC50 of around 100 µM. This is the concentration the cells were treated with before differentiation in the metabolomics experiment yet most metabolites don't show decreased levels in the TBHP treated U937 group, which would be expected due to metabolic inhibition of 50% of the cells according to the MTT assays. This could mean that there is a translational issue between MTT assays and cell culture experiments with different setups. The metabolic inhibitory properties of TBHP based on the results of the MTT assays rely on the reduction to formazan by mitochondrial and non-mitochondrial reductases [77][78], therefore when looking at metabolites that are conserved in other pathways or compartments in the cell, their production doesn't necessarily have to be affected by TBHP despite the calculated IC50 value using MTT assays. Or, as previously mentioned, the underlying discrepency here could be the fast reaction time of ROS not showing any impact after 24 h let alone 7 days.

One metabolite effected by the TBHP treatment is orotic acid, which level is significantly diminished in the TBHP treated group versus the control U937 cells ($p = 1.48*10^{-6}$) (figure 39a).

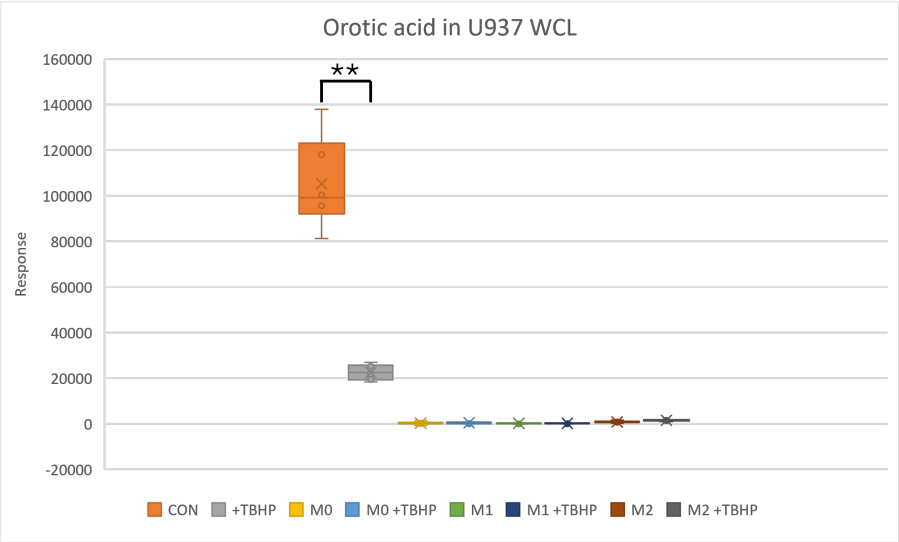

(a) Relative levels of orotic acid in six WCL replicates of U937 cells, M0-, M1- and M2 macrophages treated with and without 100 µM TBHP. ** $p < 0.001$

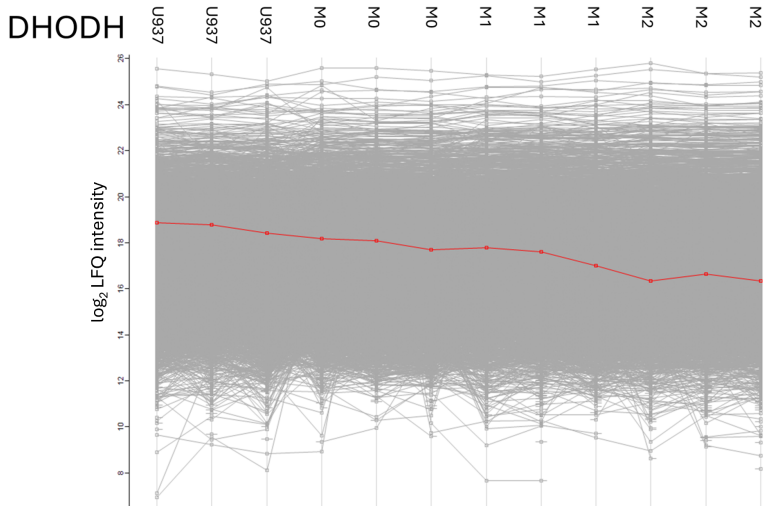

(b) Profile plot of DHODH $\log_2$ LFQ intensity values of three replicates of each of the U937 differentiation states

Figure 39: Relative levels of orotic acid in WCL of U937 cells, M0-, M1- and M2 macrophages treated with and without TBHP as well as DHODH in WCL of all cell types

Orotic acid is used in the biosynthesis of pyrimidine nucleobases [79], which would explain the high signal in undifferentiated U937 cells (figure 39a) and the overexpression of the synthesizing enzyme dihydroorotate dehydrogenase (DHODH) (figure 39b), since these cells divide rapidly. Yet this cellular function of division could be susceptible to ROS damage which therefore leads to lower production of orotic acid when cells are put under oxidative stress. Since the enzyme that produces orotic acid, DHODH, is a mitochondrial enzyme [80] it's function might be hindered by the mitochondrial damaging nature of TBHP [44]. Yet interestingly the level of uridine 5-monophosphate (UMP), which is a nucleotide synthesized from orotic acid [79], is not decreased in the TBHP treated U937 group (figure 40a). The U937 cells have overall higher levels of this nucleotide compared to the differentiated macrophages, which coincides with the higher expression of the synthesizing enzyme uridine 5-monophosphate synthase (UMPS) (figure 40c). Additionally, M0- and M1 macrophages seem to secrete this nucleotide as it is found in their respective supernatants (figure 40b).

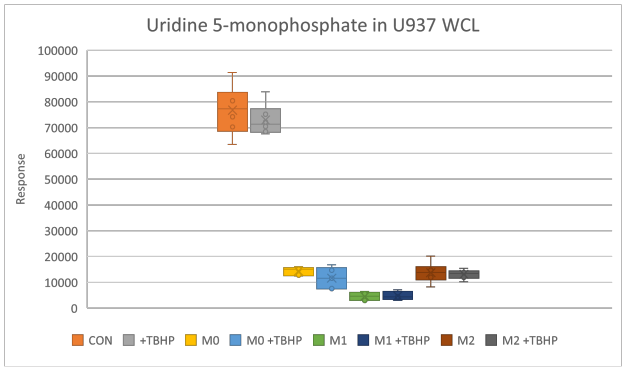

(a) Relative levels of UMP in six WCL replicates of U937 cells, M0-, M1- and M2 macrophages treated with and without 100 µM TBHP

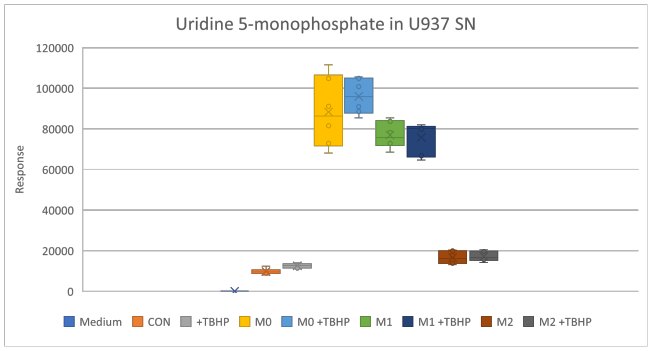

(b) Relative levels of UMP in six SN replicates of U937 cells, M0-, M1- and M2 macrophages treated with and without 100 µM TBHP as well as base level in medium

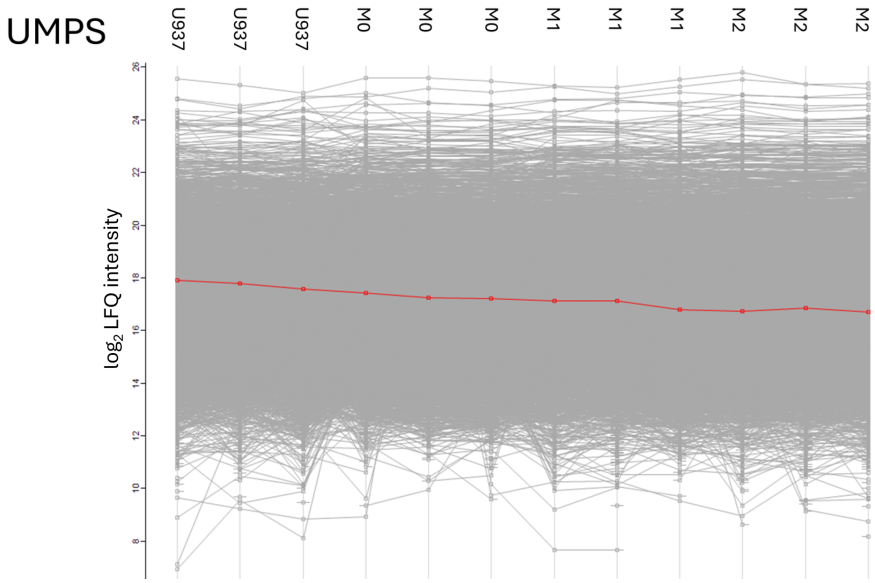

(c) Profile plot of UMPS $\log_2$ LFQ intensity values of three replicates of each of the U937 differentiation states

Figure 40: Relative amounts of UMP in WCL and SN of U937 cells, M0-, M1- and M2 macrophages treated with and without TBHP as well as UMPS in WCL of all cell types

Another metabolite affected by the TBHP treatment is 3-HAA, which is present at a significantly higher level in the SN of the M1 group treated with TBHP relative to the untreated M1 cells (p =

$7.99*10^{-3}$) (figure 25a). 3-HAA has been described as having a two sided behavior concerning ROS as it can act as a antioxidant by scavenging free radicals and inducing antioxidant genes, on the other hand it is able to promote hydroxyl radical formation in the presence of certain metal ions [81][82].
It has been described that ROS can up-regulate glycolysis in certain cells [83] and as previously mentioned, macrophages under oxidative stress are rewired to promote glycolysis, which is used to regulate M1 polarization [8][10][31]. Fitting this notion, the level of the glycolysis intermediate DHAP is significantly increased in the M1-like cells treated with TBHP compared to the untreated M1 macrophages ($p = 2.62*10^{-3}$) (figures 26). While not significantly increased, the other glycolysis intermediate fructose-1,6-biphosphate follows the same trend (figure 27).

5 Conclusion

The method applied here to differentiate U937 cells into M0-, M1- and M2-like macrophages and subsequently analyze their metabolome using ion-pairing triple quadrupole LC-MS allowed for clear differences of the macrophage polarization states to be observed. These hallmarks in the metabolomes of the different cell types were confirmed with the expression profiles of proteins correlated with the respective pathways. This highlights the robustness of the performed metabolomics and proteomics analysis. The findings here also underline the plasticity of macrophage polarization and how it is to be seen as a gradient, where the M1 and M2 state merely representing two extremes on opposing ends, with cells being able to functionally be somewhere in between those two states. This means that certain metabolic pathways don't solely occur in macrophages of one type and pro- and anti-inflammatory pathways can be found in the same cell. TBHP treatment of cells before differentiation showed effect on specific metabolites that are implicated in cellular ROS homeostasis as well as localized in compartments damaged by oxidative stress. These experiments give deeper insight into the metabolism of the differently polarized macrophages, therefore acting as progress towards understanding macrophage polarization. This forms the basis for the future development of novel cancer therapies that benefit from this phenomenon.

6 References

[1] Chen Varol, Alexander Mildner, and Steffen Jung. "Macrophages: Development and Tissue Specialization". In: *Annual Review of Immunology* 33 (Mar. 2015). Publisher: Annual Reviews, pp. 643–675. ISSN: 0732-0582, 1545-3278. DOI: 10.1146/annurev-immunol-032414-112220.

[2] Jr Charles A Janeway et al. "Principles of innate and adaptive immunity". In: *Immunobiology: The Immune System in Health and Disease. 5th edition*. Garland Science, 2001.

[3] Florent Ginhoux and Martin Guilliams. "Tissue-Resident Macrophage Ontogeny and Homeostasis". In: *Immunity* 44.3 (Mar. 2016), pp. 439–449. ISSN: 10747613. DOI: 10.1016/j.immuni.2016.02.024.

[4] Nagatoshi Fujiwara and Kazuo Kobayashi. "Macrophages in Inflammation". In: *Current Drug Targets - Inflammation & Allergy* 4.3 (June 2005), pp. 281–286. DOI: 10.2174/1568010054022024.

[5] Stephen J. Jenkins and Judith E. Allen. "The expanding world of tissue-resident macrophages". In: *European Journal of Immunology* 51.8 (2021), pp. 1882–1896. ISSN: 1521-4141. DOI: 10.1002/eji.202048881.

[6] Abbas Shapouri-Moghaddam et al. "Macrophage plasticity, polarization, and function in health and disease". In: *Journal of Cellular Physiology* 233.9 (Sept. 2018), pp. 6425–6440. ISSN: 0021-9541, 1097-4652. DOI: 10.1002/jcp.26429.

[7] Yoshitake Desaki et al. "Bacterial lipopolysaccharides induce defense responses associated with programmed cell death in rice cells". In: *Plant & Cell Physiology* 47.11 (Nov. 2006), pp. 1530–1540. ISSN: 0032-0781. DOI: 10.1093/pcp/pcl019.

[8] Salvador Pérez and Sergio Rius-Pérez. "Macrophage Polarization and Reprogramming in Acute Inflammation: A Redox Perspective". In: *Antioxidants* 11.7 (July 2022), p. 1394. ISSN: 2076-3921. DOI: 10.3390/antiox11071394.

[9] Ping Wang et al. "Macrophage achieves self-protection against oxidative stress-induced ageing through the Mst-Nrf2 axis". In: *Nature Communications* 10.1 (Feb. 2019). Publisher: Nature Publishing Group, p. 755. ISSN: 2041-1723. DOI: 10.1038/s41467-019-08680-6.

[10] László Virág et al. "Self-defense of macrophages against oxidative injury: Fighting for their own survival". In: *Redox Biology* 26 (June 2019). ISSN: 2213-2317. DOI: 10.1016/j.redox.2019.101261.

[11] Brandon Griess et al. "Scavenging reactive oxygen species selectively inhibits M2 macrophage polarization and their pro-tumorigenic function in part, via Stat3 suppression". In: *Free Radical Biology and Medicine* 147 (Feb. 2020), pp. 48–60. ISSN: 08915849. DOI: 10.1016/j.freeradbiomed.2019.12.018.

[12] Marcella Canton et al. "Reactive Oxygen Species in Macrophages: Sources and Targets". In: *Frontiers in Immunology* 12 (Sept. 2021). ISSN: 1664-3224. DOI: 10.3389/fimmu.2021.734229.

[13] Juhi Bagaitkar et al. "NADPH oxidase activation regulates apoptotic neutrophil clearance by murine macrophages". In: *Blood* 131.21 (May 2018), pp. 2367–2378. ISSN: 0006-4971. DOI: 10.1182/blood-2017-09-809004.

[14] Bingtao Zhang et al. "Efferocytosis: the resolution of inflammation in cardiovascular and cerebrovascular disease". In: *Frontiers in Immunology* 15 (2024). ISSN: 1664-3224. DOI: 10.3389/fimmu.2024.1485222.

[15] Prabhash Kumar Jha, Masanori Aikawa, and Elena Aikawa. "Macrophage Heterogeneity and Efferocytosis: Beyond the M1/M2 Dichotomy". In: *Circulation Research* 134.2 (Jan. 2024). Publisher: American Heart Association, pp. 186–188. DOI: 10.1161/CIRCRESAHA.123.324011.

[16] YuLing Zhang, Hongjing Zang, and Qiuyuan Wen. "Macrophage polarization in tumors: The impact of efferocytosis". In: *International Immunopharmacology* 168 (Jan. 2026). ISSN: 15675769. DOI: 10.1016/j.intimp.2025.115807.

[17] Yan Zhang et al. “ROS play a critical role in the differentiation of alternatively activated macrophages and the occurrence of tumor-associated macrophages”. In: *Cell Research* 23.7 (July 2013). Publisher: Nature Publishing Group, pp. 898–914. ISSN: 1748-7838. DOI: 10.1038/cr.2013.75.

[18] Lei Wang et al. “Promoting macrophage phagocytosis of cancer cells for effective cancer immunotherapy”. In: *Biochemical Pharmacology* 232 (Feb. 2025). ISSN: 00062952. DOI: 10.1016/j.bcp.2024.116712.

[19] Jon Zugazagoitia et al. “Current Challenges in Cancer Treatment”. In: *Clinical Therapeutics* 38.7 (July 2016), pp. 1551–1566. ISSN: 01492918. DOI: 10.1016/j.clinthera.2016.03.026.

[20] Douglas Hanahan and Robert A. Weinberg. “Hallmarks of Cancer: The Next Generation”. In: *Cell* 144.5 (Mar. 2011), pp. 646–674. ISSN: 00928674. DOI: 10.1016/j.cell.2011.02.013.

[21] Dmitriy Sonkin, Anish Thomas, and Beverly A. Teicher. “Cancer treatments: Past, present, and future”. In: *Cancer Genetics* 286-287 (Aug. 2024), pp. 18–24. ISSN: 22107762. DOI: 10.1016/j.cancergen.2024.06.002.

[22] Astrid Slany et al. “Targeting breast cancer-associated fibroblasts to improve anti-cancer therapy”. In: *The Breast* 24.5 (Oct. 2015), pp. 532–538. ISSN: 09609776. DOI: 10.1016/j.breast.2015.06.009.

[23] Ava J. Boutilier and Sherine F. Elsawa. “Macrophage Polarization States in the Tumor Microenvironment”. In: *International Journal of Molecular Sciences* 22.13 (June 2021). ISSN: 1422-0067. DOI: 10.3390/ijms22136995.

[24] Xing-Qing Pan. “The mechanism of the anticancer function of M1 macrophages and their use in the clinic”. In: *Chinese Journal of Cancer* (Nov. 2012). ISSN: 1000467X, 1944446X. DOI: 10.5732/cjc.012.10046.

[25] Olga V. Kovaleva et al. “M1 macrophages – unexpected contribution to tumor progression”. In: *Frontiers in Immunology* 16 (July 2025). ISSN: 1664-3224. DOI: 10.3389/fimmu.2025.1638102.

[26] Elise Hickman et al. “Expanded characterization of in vitro polarized M0, M1, and M2 human monocyte-derived macrophages: Bioenergetic and secreted mediator profiles”. In: *PLOS ONE* 18.3 (Mar. 2023). ISSN: 1932-6203. DOI: 10.1371/journal.pone.0279037.

[27] *U-937 - CRL-1593.2 — ATCC*. URL: https://www.atcc.org/products/crl-1593.2 (visited on 10/24/2025).

[28] Johannes J. Kovarik et al. “A multi-omics based anti-inflammatory immune signature characterizes long COVID-19 syndrome”. In: *iScience* 26.1 (Dec. 2022). ISSN: 2589-0042. DOI: 10.1016/j.isci.2022.105717.

[29] Fernando O. Martinez and Siamon Gordon. “The M1 and M2 paradigm of macrophage activation: time for reassessment”. In: *F1000Prime Reports* 6 (Mar. 2014). ISSN: 20517599. DOI: 10.12703/P6-13.

[30] Kangling Zhang, Abhishek Mishra, and Chinnaswamy Jagannath. “New insight into arginine and tryptophan metabolism in macrophage activation during tuberculosis”. In: *Frontiers in Immunology* 15 (Apr. 2024). Publisher: Frontiers. ISSN: 1664-3224. DOI: 10.3389/fimmu.2024.1363938.

[31] Pengzhen Zhuang et al. “Regulating macrophage glucose metabolism homeostasis via mitochondrial rheostats by short fiber-microsphere scaffolds for bone repair”. In: *Bioactive Materials* 49 (July 2025), pp. 399–417. ISSN: 2452-199X. DOI: 10.1016/j.bioactmat.2025.03.008.

[32] Stefanie K. Wculek et al. “Metabolism of tissue macrophages in homeostasis and pathology”. In: *Cellular & Molecular Immunology* 19.3 (Mar. 2022). Publisher: Nature Publishing Group, pp. 384–408. ISSN: 2042-0226. DOI: 10.1038/s41423-021-00791-9.

[33] Antonella Viola et al. “The Metabolic Signature of Macrophage Responses”. In: *Frontiers in Immunology* 10 (July 2019), p. 1462. ISSN: 1664-3224. DOI: 10.3389/fimmu.2019.01462.

[34] Ana Batista-Gonzalez et al. “New Insights on the Role of Lipid Metabolism in the Metabolic Reprogramming of Macrophages”. In: *Frontiers in Immunology* 10 (Jan. 2020). ISSN: 1664-3224. DOI: 10.3389/fimmu.2019.02993.

[35] William J. Griffiths and Yuqin Wang. "Mass spectrometry: from proteomics to metabolomics and lipidomics". In: *Chemical Society Reviews* 38.7 (2009), p. 1882. ISSN: 0306-0012, 1460-4744. DOI: 10.1039/b618553n.

[36] Jan Ståhlberg. "Retention models for ions in chromatography". In: *Journal of Chromatography A* 855.1 (Sept. 1999), pp. 3–55. ISSN: 00219673. DOI: 10.1016/S0021-9673(99)00176-4.

[37] Hartmut Schlüter. "Reversed-Phase Chromatography". In: *Journal of Chromatography Library*. Vol. 61. ISSN: 0301-4770. Elsevier, Jan. 2000, pp. 147–234. DOI: 10.1016/S0301-4770(08)60531-X.

[38] Jürgen H. Gross. *Mass Spectrometry: A Textbook*. Berlin, Heidelberg: Springer Berlin Heidelberg, 2011. ISBN: 978-3-642-10709-2. DOI: 10.1007/978-3-642-10711-5.

[39] Florian Meier et al. "Parallel Accumulation–Serial Fragmentation (PASEF): Multiplying Sequencing Speed and Sensitivity by Synchronized Scans in a Trapped Ion Mobility Device". In: *Journal of Proteome Research* 14.12 (Dec. 2015), pp. 5378–5387. ISSN: 1535-3893, 1535-3907. DOI: 10.1021/acs.jproteome.5b00932.

[40] Peter Stone et al. "New Dynamic MRM Mode Improves Data Quality and Triple Quad Quantification in Complex Analyses". In: *Agilent publication 5990-3595EN* (June 2009).

[41] Jürgen Cox and Matthias Mann. "MaxQuant enables high peptide identification rates, individualized p.p.b.-range mass accuracies and proteome-wide protein quantification". In: *Nature Biotechnology* 26.12 (Dec. 2008), pp. 1367–1372. ISSN: 1546-1696. DOI: 10.1038/nbt.1511.

[42] Stefka Tyanova et al. "The Perseus computational platform for comprehensive analysis of (prote)omics data". In: *Nature Methods* 13.9 (Sept. 2016), pp. 731–740. ISSN: 1548-7105. DOI: 10.1038/nmeth.3901.

[43] Celia Andrés Juan et al. "The Chemistry of Reactive Oxygen Species (ROS) Revisited: Outlining Their Role in Biological Macromolecules (DNA, Lipids and Proteins) and Induced Pathologies". In: *International Journal of Molecular Sciences* 22.9 (Apr. 2021). ISSN: 1422-0067. DOI: 10.3390/ijms22094642.

[44] Kanupriya et al. "Mechanism of tert-butylhydroperoxide induced cytotoxicity in U-937 macrophages by alteration of mitochondrial function and generation of ROS". In: *Toxicology in Vitro* 21.5 (Aug. 2007), pp. 846–854. ISSN: 08872333. DOI: 10.1016/j.tiv.2007.02.007.

[45] *UniProt*. URL: https://www.uniprot.org/uniprotkb/P11215/entry (visited on 11/14/2025).

[46] Alexandra Nikonova et al. "M1-like macrophages are potent producers of anti-viral interferons and M1-associated marker-positive lung macrophages are decreased during rhinovirus-induced asthma exacerbations". In: *EBioMedicine* 54 (Apr. 2020). ISSN: 23523964. DOI: 10.1016/j.ebiom.2020.102734.

[47] Ruolan Li et al. "LPS-induced PTGS2 manipulates the inflammatory response through trophoblast invasion in preeclampsia via NF-κB pathway". In: *Reproductive Biology* 22.4 (Dec. 2022). ISSN: 1642431X. DOI: 10.1016/j.repbio.2022.100696.

[48] Yongli Yao, Xiang-Hong Xu, and Liping Jin. "Macrophage Polarization in Physiological and Pathological Pregnancy". In: *Frontiers in Immunology* 10 (Apr. 2019), p. 792. ISSN: 1664-3224. DOI: 10.3389/fimmu.2019.00792.

[49] Tamás Rőszer. "Understanding the Mysterious M2 Macrophage through Activation Markers and Effector Mechanisms". In: *Mediators of Inflammation* 2015.1 (Jan. 2015). Ed. by Yona Keisari. ISSN: 0962-9351, 1466-1861. DOI: 10.1155/2015/816460.

[50] Yutao Wang et al. "M2 Macrophage Co-Expression Factors Correlate With Immune Phenotype and Predict Prognosis of Bladder Cancer". In: *Frontiers in Oncology* 11 (Mar. 2021). ISSN: 2234-943X. DOI: 10.3389/fonc.2021.609334.

[51] Tanja Buchacher et al. "M2 Polarization of Human Macrophages Favors Survival of the Intracellular Pathogen Chlamydia pneumoniae". In: *PLOS ONE* 10.11 (Nov. 2015). Ed. by Ashlesh K Murthy. ISSN: 1932-6203. DOI: 10.1371/journal.pone.0143593.

[52] Kyoungran Lee, Jong-Hwan Kwak, and Suhkneung Pyo. "Inhibition of LPS-induced inflammatory mediators by 3-hydroxyanthranilic acid in macrophages through suppression of PI3K/NF-κB signaling pathways". In: *Food & Function* 7.7 (July 2016). Publisher: The Royal Society of Chemistry, pp. 3073–3082. ISSN: 2042-650X. DOI: 10.1039/C6FO00187D.

[53] Ahmed Sadik et al. "IL4I1 Is a Metabolic Immune Checkpoint that Activates the AHR and Promotes Tumor Progression". In: *Cell* 182.5 (Sept. 2020), pp. 1252–1270. ISSN: 00928674. DOI: 10.1016/j.cell.2020.07.038.

[54] S. R. Thomas and R. Stocker. "Antioxidant activities and redox regulation of interferon-gamma-induced tryptophan metabolism in human monocytes and macrophages". In: *Advances in Experimental Medicine and Biology* 467 (1999), pp. 541–552. ISSN: 0065-2598. DOI: 10.1007/978-1-4615-4709-9_67.

[55] Yinpu Yue et al. "IL4I1 Is a Novel Regulator of M2 Macrophage Polarization That Can Inhibit T Cell Activation via L-Tryptophan and Arginine Depletion and IL-10 Production". In: *PLOS ONE* 10.11 (Nov. 2015). Publisher: Public Library of Science. ISSN: 1932-6203. DOI: 10.1371/journal.pone.0142979.

[56] Tai Huang et al. "Indole-3-pyruvic acid alleviates rheumatoid arthritis via the aryl hydrocarbon receptor pathway". In: *Annals of Translational Medicine* 11.5 (Mar. 2023), p. 213. ISSN: 2305-5839. DOI: 10.21037/atm-23-1074.

[57] Linxuan Xue et al. "Tryptophan metabolism regulates inflammatory macrophage polarization as a predictive factor for breast cancer immunotherapy". In: *International Immunopharmacology* 125 (Dec. 2023). ISSN: 15675769. DOI: 10.1016/j.intimp.2023.111196.

[58] *KEGG PATHWAY: Tryptophan metabolism - Homo sapiens (human)*. URL: https://www.kegg.jp/pathway/hsa00380+8942 (visited on 11/06/2025).

[59] Ana S. López et al. "Effect of 3-hydroxyanthranilic acid in the immunosuppressive molecules indoleamine dioxygenase and HLA-G in macrophages". In: *Immunology Letters* 117.1 (Apr. 2008), pp. 91–95. ISSN: 01652478. DOI: 10.1016/j.imlet.2008.01.001.

[60] Heiko Mühl and Josef Pfeilschifter. "Anti-inflammatory properties of pro-inflammatory interferon-gamma". In: *International Immunopharmacology* 3.9 (Sept. 2003), pp. 1247–1255. ISSN: 1567-5769. DOI: 10.1016/S1567-5769(03)00131-0.

[61] K. Watcharanurak et al. "Effects of upregulated indoleamine 2, 3-dioxygenase 1 by interferon γ gene transfer on interferon γ-mediated antitumor activity". In: *Gene Therapy* 21.9 (Sept. 2014), pp. 794–801. ISSN: 1476-5462. DOI: 10.1038/gt.2014.54.

[62] Mengyuan Li et al. "Metabolism, metabolites, and macrophages in cancer". In: *Journal of Hematology & Oncology* 16.1 (July 2023), p. 80. ISSN: 1756-8722. DOI: 10.1186/s13045-023-01478-6.

[63] D.L. Nelson and M.M. Cox. *Lehninger Principles of Biochemistry: 6th Edition*. Macmillan Learning, 2012. ISBN: 978-1-4641-0962-1.

[64] L Jin, G N Alesi, and S Kang. "Glutaminolysis as a target for cancer therapy". In: *Oncogene* 35.28 (July 2016), pp. 3619–3625. ISSN: 0950-9232, 1476-5594. DOI: 10.1038/onc.2015.447.

[65] Markus Kieler, Melanie Hofmann, and Gernot Schabbauer. "More than just protein building blocks: how amino acids and related metabolic pathways fuel macrophage polarization". In: *The FEBS Journal* 288.12 (2021), pp. 3694–3714. ISSN: 1742-4658. DOI: 10.1111/febs.15715.

[66] Zhou Ji et al. "The malic acid inhibiting inflammation in ankylosing spondylitis by interfering M1 macrophage polarization". In: *International Immunopharmacology* 144 (Jan. 2025). ISSN: 1567-5769. DOI: 10.1016/j.intimp.2024.113653.

[67] Fang-Ling Zhang et al. "Organoids transplantation attenuates intestinal ischemia/reperfusion injury in mice through L-Malic acid-mediated M2 macrophage polarization". In: *Nature Communications* 14.1 (Oct. 2023). ISSN: 2041-1723. DOI: 10.1038/s41467-023-42502-0.

[68] Puneet Gaitonde, Vivek S. Purohit, and Sathy V. Balu-Iyer. "Intravenous administration of Factor VIII–O-Phospho-L-Serine (OPLS) complex reduces immunogenicity and preserves pharmacokinetics of the therapeutic protein". In: *European Journal of Pharmaceutical Sciences* 66 (Jan. 2015), pp. 157–162. ISSN: 0928-0987. DOI: 10.1016/j.ejps.2014.10.010.

[69] Xiaohua Ma et al. "Phosphatidylserine, inflammation, and central nervous system diseases". In: *Frontiers in Aging Neuroscience* 14 (Aug. 2022). Publisher: Frontiers. ISSN: 1663-4365. DOI: 10.3389/fnagi.2022.975176.

[70] Wenting He et al. "Vitamin B5 Reduces Bacterial Growth via Regulating Innate Immunity and Adaptive Immunity in Mice Infected with Mycobacterium tuberculosis". In: *Frontiers in Immunology* 9 (Feb. 2018), p. 365. ISSN: 1664-3224. DOI: 10.3389/fimmu.2018.00365.

[71] Hongqiao Zhang and Henry Jay Forman. "Glutathione synthesis and its role in redox signaling". In: *Seminars in cell & developmental biology* 23.7 (Sept. 2012), pp. 722–728. ISSN: 1084-9521. DOI: 10.1016/j.semcdb.2012.03.017.

[72] Pietro Ghezzi. "Role of glutathione in immunity and inflammation in the lung". In: *International Journal of General Medicine* 4 (Jan. 2011), pp. 105–113. ISSN: null. DOI: 10.2147/IJGM.S15618.

[73] Yang Yang et al. "γ-glutamylcysteine exhibits anti-inflammatory effects by increasing cellular glutathione level". In: *Redox Biology* 20 (Jan. 2019), pp. 157–166. ISSN: 2213-2317. DOI: 10.1016/j.redox.2018.09.019.

[74] Hongqiao Zhang et al. "Down regulation of glutathione and glutamate cysteine ligase in the inflammatory response of macrophages". In: *Free Radical Biology and Medicine* 158 (Oct. 2020), pp. 53–59. ISSN: 0891-5849. DOI: 10.1016/j.freeradbiomed.2020.06.017.

[75] *UniProt*. URL: https://www.uniprot.org/uniprotkb/P07203/entry (visited on 11/18/2025).

[76] *UniProt*. URL: https://www.uniprot.org/uniprotkb/P04179/entry (visited on 11/18/2025).

[77] M. V. Berridge and A. S. Tan. "Characterization of the Cellular Reduction of 3-(4,5-dimethylthiazol-2-yl)-2,5-diphenyltetrazolium bromide (MTT): Subcellular Localization, Substrate Dependence, and Involvement of Mitochondrial Electron Transport in MTT Reduction". In: *Archives of Biochemistry and Biophysics* 303.2 (June 1993), pp. 474–482. ISSN: 0003-9861. DOI: 10.1006/abbi.1993.1311.

[78] N.T.H. Nga et al. "Optimization and application of MTT assay in determining density of suspension cells". In: *Analytical Biochemistry* 610 (Dec. 2020). ISSN: 00032697. DOI: 10.1016/j.ab.2020.113937.

[79] Valerie Walker. "Ammonia Metabolism and Hyperammonemic Disorders". In: *Advances in Clinical Chemistry*. Vol. 67. ISSN: 0065-2423. Elsevier, Jan. 2014, pp. 73–150. DOI: 10.1016/bs.acc.2014.09.002.

[80] *UniProt*. URL: https://www.uniprot.org/uniprotkb/Q02127/entry (visited on 11/18/2025).

[81] Daniela Krause et al. "The Tryptophan Metabolite 3-Hydroxyanthranilic Acid Plays Anti-Inflammatory and Neuroprotective Roles During Inflammation". In: *The American Journal of Pathology* 179.3 (Sept. 2011), pp. 1360–1372. ISSN: 0002-9440. DOI: 10.1016/j.ajpath.2011.05.048.

[82] Adriana Pérez-González, Juan Raúl Alvarez-Idaboy, and Annia Galano. "Dual antioxidant/pro-oxidant behavior of the tryptophan metabolite 3-hydroxyanthranilic acid: a theoretical investigation of reaction mechanisms and kinetics". In: *New Journal of Chemistry* 41.10 (May 2017). Publisher: The Royal Society of Chemistry, pp. 3829–3845. ISSN: 1369-9261. DOI: 10.1039/C6NJ03980D.

[83] Dong-yun Shi et al. "The role of cellular oxidative stress in regulating glycolysis energy metabolism in hepatoma cells". In: *Molecular Cancer* 8 (June 2009), p. 32. ISSN: 1476-4598. DOI: 10.1186/1476-4598-8-32.

7 Appendix

Table 10: Composition of standard peptide mix from Peptide Specialty Laboratories GmbH used for proteomics LC-MS measurements and analysis

Peptid 1-2 mg M28: TTPAVLDSDGSYFLYSK
Peptid 1-2 mg HK0: VLETKSLYVR
Peptid 1-2 mg HK1: VLETK(e-AC)SLYVR

Table 11: Modified Agilent metabolomics LC-MS dMRM method

Compound Name	Precursor Ion	Product Ion	Ret Time (min)	Δ Ret Time	Collision Energy
2-2-Dimethyl Succinic acid	145.1	127.1	14	4	8
2-2-Dimethyl Succinic acid	145.1	101.1	14	4	11
2-3-Pyridinedicarboxylic acid	166	122	14.9	2	6
2-3-Pyridinedicarboxylic acid	166	78.1	14.9	2	13
2-Deoxyadenosine	310.1	250	6.5	4	4
2-Deoxyadenosine	250	134.05	6.5	4	12
2-Deoxyadenosine 5-monophosphate	330	134.05	12.7	4	28
2-Deoxyadenosine 5-monophosphate	330	79	12.7	4	48
2-Deoxycytidine 5-diphosphate	386	97	15	4	20
2-Deoxycytidine 5-diphosphate	386	79	15	4	36
2-Deoxy-D-ribose	193.1	133	1.4	2	0
2-Deoxy-D-ribose	193.1	59.2	1.4	2	16
2-Deoxyguanosine 5-diphosphate	426	158.9	15.4	2	28
2-Deoxyguanosine 5-diphosphate	426	79.1	15.4	2	48
2-Deoxyguanosine 5-monophosphate	346	97	12	4	36
2-Deoxyguanosine 5-monophosphate	346	79.1	12	4	48
2-Deoxyinosine	251.1	135	3.7	2	20
2-Deoxyinosine	251.1	108	3.7	2	42
2-Deoxyuridine	227.1	184	2.3	3	6
2-Deoxyuridine	227.1	42.2	2.3	3	20
2-Isopropylmalic acid	175.1	115	15.5	4	13
2-Isopropylmalic acid	175.1	113	15.5	4	13
2-Methyl-1-butanol	87.1	43.3	9.6	4	5
2-Phosphoglyceric acid	185	97	14.8	4	14
2-Phosphoglyceric acid	185	79	14.8	4	37
3-2-Hydroxyethylindole	160.1	142.07	15.4	2	16
3-2-Hydroxyethylindole	160.1	130.06	15.4	2	14
3-Hydroxyanthranilic acid	152	108	12.1	2	12
3-Hydroxyanthranilic acid	152	107	12.1	2	23
3-Hydroxy-DL-kynurenine	223.1	205.9	2	2	4
3-Hydroxy-DL-kynurenine	223.1	162	2	2	10
3-Hydroxyphenylacetic acid	151	107.1	14.2	2	4
3-Hydroxyphenylacetic acid	151	65.2	14.2	2	26
3-Indoleacetic acid	174.1	130	16.5	4	7
3-Indoleacetic acid	174.1	128	16.5	4	19
3-Methylglutaric acid	145.1	101.1	14.1	2	11
3-Methylglutaric acid	145.1	41.3	14.1	2	52
4-Aminobenzoic acid	136	92	9.5	2	8
4-Hydroxy-L-glutamic acid	162	144	4.1	4	6
4-Hydroxy-L-glutamic acid	162	72.1	4.1	4	16
4-Hydroxyphenyl-pyruvic acid	179	107	14.7	4	4
4-Methyl-2-oxovaleric acid	129.1	85.1	13.7	2	7
4-Pyridoxic acid	182	138	15.3	2	12
4-Pyridoxic acid	182	108.1	15.3	2	20
5-Deoxy-5-(methylthio)adenosine	356.1	296	11.8	2	4
5-Deoxy-5-(methylthio)adenosine	356.1	134	11.8	2	12
5-Hydroxy-3-indoleacetic acid	190.1	144	13	2	21
5-Hydroxy-3-indoleacetic acid	190.1	116	13	2	46

Acetyl-CoA	809.2	728.1	18.4	4	15
Acetyl-CoA	809.2	461.1	18.4	4	15
Acetyl-CoA	809.2	408.2	18.4	4	10
Adenine	134	107	2.8	2	18
Adenine	134	92.1	2.8	2	20
Adenosine	326.1	134	6.4	2	20
Adenosine	266	134	6.4	2	10
Adenosine 3-5-cyclic monophosphate	328	134	13.4	2	24
Adenosine 3-5-cyclic monophosphate	328	79	13.4	2	48
Adenosine 5-diphosphate	426	328	15.4	2	16
Adenosine 5-diphosphate	426	159	15.4	2	28
Adenosine 5-monophosphate	346	97	12	4	24
Adenosine 5-monophosphate	346	79	12	4	38
Adenosine 5-triphosphate	506	408.1	17.2	4	22
Adenosine 5-triphosphate	506	159	17.2	4	38
Adipic acid	145.1	101.1	14.3	2	11
Adipic acid	145.1	83.1	14.3	2	12
AICAR	257.1	125	2	2	10
AICAR	257.1	42.2	2	2	44
Allantoin	157	97	1.3	2	12
Allantoin	157	42.2	1.3	2	16
alpha-D-Glucose-1-phosphate	259	240.9	7.6	5	9
alpha-D-Glucose-1-phosphate	259	79	7.6	5	28
alpha-Ketoglutaric acid	145	101	14.3	3	5
alpha-Ketoglutaric acid	145	57.2	14.3	3	9
alpha-Ketoglutaric acid-C13	146.1	102.1	14.3	2	5
alpha-Ketoglutaric acid-C13	146.1	57	14.3	2	10
Anthranilic acid	136.1	92.1	14.9	2	15
Anthranilic acid	136.1	65.1	14.9	2	40
Arabinose-5-phosphate	229	97	8.4	4	8
Arabinose-5-phosphate	229	79	8.4	4	36
Argininosuccinic acid	289	131.1	5.1	4	27
Argininosuccinic acid	289	88	5.1	4	36
beta-Nicotinamide adenine dinucleotide	662.1	540	9.5	2	12
beta-Nicotinamide adenine dinucleotide	662.1	327.9	9.5	2	36
beta-Nicotinamide mononucleotide	333	251.1	3.7	2	12
beta-Nicotinamide mononucleotide	333	135.1	3.7	2	36
Cellobiose	341.1	161	1.3	2	5
cis-Aconitic acid	173	129	15.5	2	4
cis-Aconitic acid	173	85.1	15.5	2	8
Citramalic acid	147	87	13.8	3	14
Citramalic acid	147	85.1	13.8	3	12
Citric acid	191	111.01	14.9	4	10
Citric acid	191	87.01	14.9	4	16
Creatine	130.1	88.1	1.3	2	8
Creatine	130.1	41.2	1.3	2	36
Creatine phosphate	210	96.9	7	2	4
Creatine phosphate	210	79	7	2	16
Creatinine	112	68.1	1.35	2	16
Creatinine	112	41.2	1.35	2	24
Cytidine	242.1	109	1.8	2	8
Cytidine	242.1	42.2	1.8	2	16
Cytidine 5-diphosphate	402.01	158.92	14.4	2	24
Cytidine 5-diphosphate	402.01	79	14.4	2	48
Cytidine 5-triphosphate	482	158.8	17	3	40
Cytidine 5-triphosphate	482	79	17	3	40
Cytidine-5-monophosphate	322	97	9.7	4	22
Cytidine-5-monophosphate	322	79	9.7	4	44
Cytosine	110	67.1	1.4	2	8
Cytosine	110	42.2	1.4	2	12
D4-Succinic acid	121	102	12.8	2	10
D4-Succinic acid	121	77	12.8	2	10
D5-Kynurenic acid	193	149	15.7	2	25

D5-Kynurenic acid	193	66	15.7	2	45
Deoxyadenosine 5-triphosphate	490	391.9	17.2	3	24
Deoxyadenosine 5-triphosphate	490	158.9	17.2	3	32
Deoxycytidine 5-triphosphate	466	367.9	16.8	3	20
Deoxycytidine 5-triphosphate	466	158.9	16.8	3	28
Deoxyguanosine 5-triphosphate	506	407.9	17.2	3	20
Deoxyguanosine 5-triphosphate	506	158.8	17.2	3	32
Deoxythymidine 5-triphosphate	481	383.1	17.2	3	20
Deoxythymidine 5-triphosphate	481	158.8	17.2	3	36
D-Fructose 1,6-biphosphate	338.9	241.01	14.8	4	12
D-Fructose 1,6-biphosphate	338.9	97	14.8	4	22
D-Fructose 6-phosphate	259	97	7.6	1.5	14
D-Fructose 6-phosphate	259	79	7.6	1.5	48
D-Gluconic acid	195.1	129	5.9	4	10
D-Gluconic acid	195.1	75.2	5.9	4	18
D-Glucose 6-phosphate	259	97	7.6	4	14
D-Glucose 6-phosphate	259	79	7.6	4	48
Dihydroxyacetone phosphate	169	97	10.5	4	6
Dihydroxyacetone phosphate	169	79	10.5	4	32
DL-2-Aminoadipic acid	160.1	142	4.3	2	9
DL-2-Aminoadipic acid	160.1	116	4.3	2	12
DL-Glyceraldehyde 3-phosphate	169	97	11.7	1.5	4
DL-Glyceraldehyde 3-phosphate	169	79	11.7	1.5	28
DL-Indole-3-lactic acid	204.2	186	16.5	2	10
DL-Indole-3-lactic acid	204.2	158	16.5	2	10
DL-Indole-3-lactic acid	204.2	116	16.5	2	15
DL-Isocitric acid	191	173	15.1	4	6
DL-Isocitric acid	191	111.02	15.1	4	11
D-Mannose	179.1	89	1.3	2	4
D-Mannose	179.1	59.2	1.3	2	16
Dopamine	152	122	1.2	2	15
Dopamine	152	93.1	1.2	2	40
D-pantothenic acid	218	146.08	12.1	2	14
D-pantothenic acid	218	88	12.1	2	10
D-Ribose 5-phosphate	229	97	9	4	10
D-Ribose 5-phosphate	229	79	9	4	48
D-Ribulose 1,5-biphosphate	308.9	97	14.7	4	22
D-Ribulose 1,5-biphosphate	308.9	79	14.7	4	46
D-Sedoheptulose-7-phosphate	289	96.9	8.2	4	18
D-Sedoheptulose-7-phosphate	289	79	8.2	4	48
D-Xylose	149.05	89.02	1.2	2	4
D-Xylose	149.05	71.01	1.2	2	4
D-Xylulose-5-phosphate	229	138.98	8.5	4	8
D-Xylulose-5-phosphate	229	79	8.5	4	36
Epicatechin	289.1	245	12.2	4	11
Epicatechin	289.1	109	12.2	4	26
Flavin adenine dinucleotide	784.1	437	17	2	30
Flavin adenine dinucleotide	784.1	346	17	2	35
Galactonic acid	195.1	129	5	4	11
Galactonic acid	195.1	75.1	5	4	18
gamma-Aminobutyric acid	102	84.1	1.2	2	8
gamma-Glu-Cys	249.1	171	8.1	2	9
gamma-Glu-Cys	249.1	128	8.1	2	8
Glyceric acid	105	75.1	5.5	3	8
Glyceric acid	105	57.2	5.5	3	14
Glyoxylic acid	73	45.2	5.9	2	6
Guanine	150	133.02	2	2	12
Guanine	150	66.01	2	2	36
Guanosine	282.1	150	3.9	2	17
Guanosine	282.1	132.9	3.9	2	32
Guanosine 3,5-cyclic monophosphate	344	150.042	12.2	2	24
Guanosine 3,5-cyclic monophosphate	344	133.02	12.2	2	44
Guanosine 5-diphosphate	442	158.9	14.8	4	20

Guanosine 5-diphosphate	442	150	14.8	4	31
Guanosine 5-monophosphate	362	211	11	2	15
Guanosine 5-monophosphate	362	79	11	2	35
Guanosine 5-triphosphate	522.3	424	17	3	20
Guanosine 5-triphosphate	522.3	158.9	17	3	36
Homocitrate	205	145	15.4	2	10
Homocitrate	205	125	15.4	2	10
Hypoxanthine	135	92	2	2	17
Hypoxanthine	135	65.1	2	2	28
Indole-3-pyruvic acid	202.2	174	16.8	4	5
Indole-3-pyruvic acid	202.2	158	16.8	4	5
Indoline-2-carboxylate	162.1	118	16.1	2	11
Indoline-2-carboxylate	162.1	116	16.1	2	16
Inosine	267.1	135	3.3	2	22
Inosine	267.1	108	3.3	2	44
Inosine 5-diphosphate	427	158.9	14.5	4	28
Inosine 5-diphosphate	427	135	14.5	4	24
Inosine 5-monophosphate	347	97	11.1	2	22
Inosine 5-monophosphate	347	79	11.1	2	44
Inosine 5-triphosphate	507	409	17.2	2	19
Inosine 5-triphosphate	507	159	17.2	2	40
Isopentyl acetate	129.1	85.2	14.6	4	6
Isopentyl acetate	129.1	41.2	14.6	4	12
Itaconic acid	129	85.1	13.6	2	6
Itaconic acid	129	41.3	13.6	2	12
Ketovaleric acid	115	71.2	14.5	2	4
Kynurenic acid	188	144	15.7	2	25
Kynurenic acid	188	66	15.7	2	45
Lactic acid	89	45.3	7.4	4	9
Lactic acid	89	43.3	7.4	4	10
L-Arabinose	149	89.1	1.4	2	4
L-Arabinose	149	59.2	1.4	2	12
L-Arabitol	151	89	1.3	2	12
L-Arabitol	151	71.02	1.3	2	16
L-Arginine	173.1	156	1.1	2	8
L-Arginine	173.1	131	1.1	2	11
L-asparagine	131	113	1.2	2	4
L-asparagine	131	70	1.2	2	12
L-Aspartic Acid	132	88	4	4	10
L-Aspartic Acid	132	71	4	4	14
L-Canavanine	175.1	118	1.1	4	8
L-Canavanine	175.1	74.04	1.1	4	10
L-Carnitine	220.1	146	1.2	2	4
L-Citrulline	174.1	131	1.3	2	8
L-Citrulline	174.1	42.2	1.3	2	48
L-Cystathionine	221.1	134	1.3	2	8
L-Cystathionine	221.1	120	1.3	2	9
L-Cystine	239	120	1.2	2	4
L-Cystine	239	74.1	1.2	2	20
Levulinic acid	115.1	71	9.3	2	12
Levulinic acid	115.1	41	9.3	2	35
L-Glutamic acid	146	128	3.7	4	8
L-Glutamic acid	146	102	3.7	4	11
L-Glutamine	145.1	127	1.3	2	7
L-Glutamine	145.1	109	1.3	2	10
L-Gluthathione (oxidized)	611.1	306.07	13.6	2	24
L-Gluthathione (oxidized)	611.1	272.09	13.6	2	28
L-Histidine	154.1	137	1.1	2	12
L-Histidine	154.1	93.1	1.1	2	16
L-Homocysteine	134	116.9	1.4	2	8
L-Homocystine	267	132	1.5	2	8
L-Homocystine	267	115	1.5	2	16
L-Homoserine	118	72.1	1.3	2	10

L-Homoserine	118	55	1.3	2	16
L-Hydroxyglutaric acid	147	128.9	13.8	4	7
L-Hydroxyglutaric acid	147	85.1	13.8	4	13
Lipoamide	204.1	158	16.8	2	4
Lipoamide	204.1	64.1	16.8	2	20
Lipoamide	204.1	33.1	16.8	2	20
L-Isoleucine	130	45	2.1	2	16
L-Kynurenine	207.1	190	3.4	2	4
L-Kynurenine	207.1	144	3.4	2	20
L-Lactic acid-13C	92.1	46.1	7.4	4	10
L-Lactic acid-13C	92.1	44.1	7.4	4	10
L-Leucine	130	45	2.1	2	16
L-Malic acid	133	115	13.8	2	8
L-Malic acid	133	71.1	13.8	2	14
L-Methionine	148	100	1.8	2	6
L-Methionine	148	47.2	1.8	2	12
L-Phenylalanine	164.1	147	4	2	9
L-Phenylalanine	164.1	103	4	2	15
L-Proline	114	68.1	1.3	2	12
L-Proline	114	45.2	1.3	2	12
L-Serine	104	74.1	1.2	2	8
L-Sorbose	179.1	89	1.3	2	4
L-Sorbose	179.1	71.02	1.3	2	14
L-Threonine	118	74.1	1.3	2	9
L-Tryptophan	203.1	116	7.5	2	14
L-Tryptophan	203.1	74.1	7.5	2	14
L-Tyrosine	180	119	2.3	2	15
L-Tyrosine	180	93	2.3	2	12
Maleic acid	115	71.2	12.8	4	7
Maleic acid	115	27.3	12.8	4	15
Malonic acid	103	59.2	12.8	2	7
Malonic acid	103	41.3	12.8	2	32
Melatonine-d4	235.1	219.9	15.3	3	20
Melatonine-d4	235.1	146	15.3	3	20
Melibiose	341.1	179	1.3	2	4
Melibiose	341.1	89	1.3	2	13
Mevalonic acid	147.1	128.9	9.8	4	8
Mevalonic acid	147.1	103.1	9.8	4	11
m-Hydroxybenzoic acid	137	93.1	13.4	2	10
m-Hydroxybenzoic acid	137	65.2	13.4	2	28
myo-Inositol	239.1	179	1.3	2	0
myo-Inositol	179	71.02	1.3	2	12
N-Acetyl D-galactosamine	220.1	119	1.2	2	0
N-Acetylglutamic acid	188.1	128.04	14.1	2	10
N-Acetylglutamic acid	188.1	102	14.1	2	16
N-Acetylneuraminic acid	308.1	169.9	5.5	2	10
N-Acetylneuraminic acid	308.1	87	5.5	2	14
N-Acetyl-serotonin	217.3	157.9	9.7	4	20
N-Acetyl-serotonin	217.3	59.3	9.7	4	20
N-Acetyl-serotonine-d3	220.1	157.9	9.7	4	20
N-Acetyl-serotonine-d3	220.1	61.1	9.7	4	20
N-Carbamoyl-DL-aspartic acid	175	132	13.5	2	7
N-Carbamoyl-DL-aspartic acid	175	88.1	13.5	2	19
N-Carbamyl-L-glutamic acid	189.1	146	13.6	2	7
N-Carbamyl-L-glutamic acid	189.1	102.1	13.6	2	20
N-Formyl-L-Tyrosine	208.1	164	12.8	2	7
N-Formyl-L-Tyrosine	208.1	107	12.8	2	12
Nicotinic acid	122	78.1	11.9	4	11
Nicotinic acid	122	51.2	11.9	4	32
o-Hydroxy hippuric acid	194	150	16.5	2	11
o-Hydroxy hippuric acid	194	121	16.5	2	22
o-Phospho-L-Serine	184	97	10.2	6	13
o-Phospho-L-Serine	184	79	10.2	6	36

O-Phosphorylethanolamine	140	79	1.7	2	14
O-Phosphorylethanolamine	140	63	1.7	2	38
Orotic acid	155	42	8.8	4	26
Orotic acid	155	40	8.8	4	44
Oxamic acid	88	44.3	5.8	2	6
Oxamic acid	88	42.3	5.8	2	12
Phenol red	353.4	93	18.4	4	45
Phenol red	353.4	80	18.4	4	45
Phenylpyruvic acid	163	91.1	17.2	2	6
Phosphoenolpyruvic acid	167	79	15.3	2	12
Prephenic acid	225	101	12.4	2	9
Pyridoxal 5 phosphate	246	79	14.8	2	30
Pyridoxal hydrochloride	166.1	138	2.4	2	12
Pyridoxal hydrochloride	166.1	108	2.4	2	18
Pyridoxine	168.1	166	2.4	2	9
Pyridoxine	168.1	122.1	2.4	2	17
Pyruvic acid	87	43.2	9.5	3	4
Pyruvic acid-d4	90.1	46	9.5	3	5
Quinic acid	191.1	93.1	5.5	3	24
Quinic acid	191.1	85.1	5.5	3	25
Riboflavin	375.1	255	12.6	2	14
Riboflavin	375.1	212	12.6	2	28
S-5-Adenosyl-L-homocysteine	383.1	248	4.6	2	13
S-5-Adenosyl-L-homocysteine	383.1	134	4.6	2	24
Salicylic acid	137	93.1	16.8	1.5	17
Salicylic acid	137	65.2	16.8	1.5	33
Serotonin	175.2	144.7	15.23	2	15
Serotonin	175.2	85	15.23	2	15
Serotonin	175.2	57.1	15.23	2	15
Succinic acid	117	99	12.8	2	8
Succinic acid	117	73.1	12.8	2	10
Succinyl-CoA	866	425.8	18.4	4	30
Succinyl-CoA	866	420.3	18.4	4	25
Succinyl-CoA	866	407.9	18.4	4	35
Taurine	124	80	1.3	2	24
Taurocholic acid	514	514	20.7	2	50
Thiamine	264.1	234	1.1	2	6
Thiamine	264.1	148	1.1	2	18
Thymidine 5-diphosphate	401.01	97	15.4	4	25
Thymidine 5-diphosphate	401.01	79	15.4	4	44
Thymine	125	42.2	2.7	2	14
trans-4-Hydroxy-L-proline	130.1	128	1.3	2	12
trans-4-Hydroxy-L-proline	130.1	66.03	1.3	2	16
trans-Aconitic acid	173	129	15.55	2	4
trans-Aconitic acid	173	85.1	15.55	2	10
Uracil	111	42.2	1.7	2	14
Uric acid	167	124	4.6	2	13
Uric acid	167	42.3	4.6	2	26
Uridine	243.1	200	2.3	2	6
Uridine	243.1	110	2.3	2	12
Uridine 5-diphosphate	403	158.9	14.8	2	28
Uridine 5-diphosphate	403	79	14.8	2	48
Uridine 5'-diphosphogalactose	565	384.9	14.3	3	29
Uridine 5'-diphosphogalactose	565	322.9	14.3	3	24
Uridine 5-diphosphoglucose	565	384.9	14.3	2	28
Uridine 5-diphosphoglucose	565	322.9	14.3	2	24
Uridine 5-monophosphate	323	97	10.5	2	24
Uridine 5-monophosphate	323	79.1	10.5	2	48
Uridine 5-triphosphate	483	385	17	3	20
Uridine 5-triphosphate	483	158.9	17	3	36
Xanthine	151	108	2.1	2	16
Xanthine	151	42.2	2.1	2	24
Xanthosine	283.1	151	8.2	2	18

Xanthosine	283.1	108	8.2	2	40
Xylitol	151.1	89	1.3	2	8
Xylitol	151.1	71	1.3	2	8